POLITECNICO DI TORINO

Master's Degree in Biomedical Engineering

Politecnico di Torino

EPFL

Master's Degree Thesis

A novel computational framework to model retinal electrical stimulation

Supervisor

Prof. Valentina AGOSTINI

External supervisor

Prof. Silvestro MICERA

Candidate

Elisa AIME

Academic Year 2021/2022
December 2022

Summary

Electrical stimulation of the retina can elicit visual perceptions in patients affected by certain types of retinal degeneration by activating some of the surviving neural cells. Even though retinal prostheses are now commercially available, many conceptual and technological issues remain to be clarified. Computational modelling has contributed in the past to optimize peripheral nerve, spinal cord, and deep brain electrical stimulation, and has the potential to provide a better understanding of how the retina responds to electrical stimulation, to improve the operation of existing implants, or to propose alternative designs.

In this thesis, we developed a new computational framework to study retinal electrical stimulation. The electrical potential generated by the electrode current injection is computed through finite elements modelling (FEM) and used as input to a retinal network model where cells of different populations are modelled as point-neurons. The network model is used to compute a synaptic current, which can be applied, together with the extracellular field due to electrode current injection, to a retinal ganglion cell (RGC) morphological neuron model. Finally, the spiking activity of these RGC models is the information that reaches the visual cortex.

Our model has shown the possibility to modulate smoothly the RGCs firing rate applying different stimulation currents. It replicates known phenomena, such as the production of elongated phosphenes, but also predicts that the effect of the different populations converging to RGCs cannot be ignored when modelling the response to retinal stimulation. Finally, we show how it is possible to model the response to electrical stimulation applied at different levels in the retinal tissue, and the effect that these choices have on the retinal network activation and on the retinal output in terms of RGC firing patterns.

While our results need careful experimental validation, they pave the way for a better understanding of the interplay of the different cellular components implicated in retinal stimulation and thus to improve existing stimulation devices and techniques.

Table of Contents

List of Tables v

List of Figures vi

1 Introduction 1
- 1.1 Outline . . . 1
- 1.2 Nervous system electrophysiology . . . 2
- 1.3 Retina structure . . . 3
- 1.4 Retinal prostheses . . . 6
  - 1.4.1 Epiretinal prosthesis . . . 6
  - 1.4.2 Subretinal prosthesis . . . 7
  - 1.4.3 Suprachoroidal prosthesis . . . 7
- 1.5 Hybrid modelling . . . 7

2 Methods 9
- 2.1 Retinal network model . . . 9
  - 2.1.1 Subsampling and surface increase . . . 16
- 2.2 RGC model . . . 16
- 2.3 FEM . . . 20

3 Results 23
- 3.1 Retinal network model . . . 23
  - 3.1.1 Visual stimulation . . . 23
  - 3.1.2 Electrical stimulation . . . 23
  - 3.1.3 Subsampling . . . 27
- 3.2 RGC model . . . 27
  - 3.2.1 Point model . . . 27
  - 3.2.2 Morphological model . . . 32
- 3.3 FEM . . . 33

4 Discussion 38
4.1 Limitations 40
4.2 Future work 41

Bibliography 42

List of Tables

2.1 Values for cells position of different cell types and cells membrane characteristics. 15
2.2 Parameters used for synaptic connections 16
2.3 Initial values for RGC model 18
2.4 Rate constants equations 19
2.5 Values for RGC point model 19
2.6 Channel conductances used in the RGC morphological model 20
2.7 Layer conductivity and thickness 21
2.8 Electrode position for different implants 21

List of Figures

1.1 Typical neuron structure 3
1.2 Action potential phases over the time 4
1.3 Eye and retina structure 5
1.4 Common locations of electrode arrays in retinal prostheses 6

2.1 Flowchart of the model 10
2.2 Cell spatial distribution 11
2.3 Synaptic conductance 13
2.4 Sigmoid function to obtain RGC on and off normalized firing rate according to V_{m} 15
2.5 Cell mosaics with subsampling and surface increase 17
2.6 Retinal layers of the FEM 22

3.1 Output of visual stimulation with a dark stimulus 24
3.2 Output of visual stimulation with a bright stimulus 25
3.3 Output of visual stimulation with a checkerboard stimulus 26
3.4 Output of electric stimulation with 500 µA current 28
3.5 Difference between complete population and subsampled population (50%) after a bright visual stimulus 29
3.6 Computational time 30
3.7 Point FCM model characterization 31
3.8 Morphological FCM model characterization 32
3.9 Spiking activity changing electrode position, with increasing currents 33
3.10 Electrical stimulation of a cells grid 34
3.11 Electric potential generated through FEM, y-z plane 35
3.12 Normalized firing rate due to synaptic current for different stimulation configurations 36
3.13 Firing rate curves for different stimulation configurations 37

Chapter 1

Introduction

Electrical stimulation of the retina can elicit visual perceptions in patients affected by certain types of retinal degeneration by activating some of the surviving neural cells. Even though retinal prostheses are now commercially available, many conceptual and technological issues remain to be clarified. Computational modelling has contributed in the past to optimize peripheral nerve [1], spinal cord [2], and deep brain electrical stimulation [3], and has the potential to provide a better understanding of how the retina responds to electrical stimulation, to improve the operation of existing implants, or to propose alternative designs.

In this thesis, we developed a new computational framework to study retinal electrical stimulation. The electrical potential generated by the electrode current injection is computed through finite elements modelling (FEM) and used as input to a retinal network model where cells of different populations are modelled as point-neurons. The network model is used to compute a synaptic current, which can be applied, together with the extracellular field due to electrode current injection, to a retinal ganglion cell (RGC) morphological neuron model. Finally, the spiking activity of these RGC models is the information that reaches the visual cortex.

1.1 Outline

In the Introduction, we will first present some neuroanatomy concepts and illustrate the structure of the retina, then we will briefly describe the main retinal prostheses that have been developed. The section ends with an overview on retinal computational models proposed in literature and on hybrid modelling (HM).

In the Methods, we will describe the different components that have been implemented in our work and how they have been combined to develop the final computational framework used for the simulations. The first component is the retinal network model, the second is the RGC morphological model with its ionic

mechanism, and finally the FEM model used to compute the potential generated through electrical stimulation.

In the Results, we apply visual and electrical stimulation to the network model by Cottaris and Elfar [4] and compare our results with theirs. Additionally, we explore the idea of reducing computational complexity by substampling the retinal network. Then, we characterize the ionic mechanisms typical of RGCs in a point neuron model and in the complete RGC morphological model, both under intracellular and extracellular stimulations. The last part of the results presents the solution of the FEM model with the stimulating electrode placed in different positions in the retina, and how the surrounding cells responds to the stimulation, considering both the direct effect of extracellular electrical stimulation and the indirect effect due to synapses from the retinal network.

In the Discussion, we will comment the results obtained, the main limitation of this work and possible future directions.

1.2 Nervous system electrophysiology

The nervous system can be divided into central nervous system (CNS) and peripheral nervous system (PNS). CNS consists mainly of brain and spinal cord, while the PNS consists of the axons of the primary afferent and efferent neurons that transmit information between organs and the CNS. The retina is traditionally considered as part of the CNS. The nervous system includes two main types of cells: neurons and glial cells. Here we will only consider neurons. Neurons are excitable cell that transmit information under the form of electrical signals.

Neurons are typically composed by a soma, an axon, and a dendritic tree.

The soma is the body of the cell and contains the nucleus. Dendrites are extensions with many branches and receive information from other neurons through synapses. The axon extends from the soma and brings the information to other cells. The typical structure of a neuron can be observed in Figure 1.1.

A cell in rest condition has a different potential inside and outside the membrane, we call this difference membrane potential. Membrane potential for neurons at rest is typically between -60 and -70 mV. Membrane potential can increase or decrease in response to some events, when it moves to more positive values it's called depolarization, when it becomes more negative it's called hyperpolarization.

A neuron can transmit information generating electrical signals with variation of membrane potential. There are two main type of electrical signals that a neuron can use to communicate: action potential and graded potential.

Graded potentials are small variations of membrane potentials in response to a stimulus. The amplitude and duration of the graded potential depends on the intensity of the stimulus. A small stimulus generates a small change in membrane

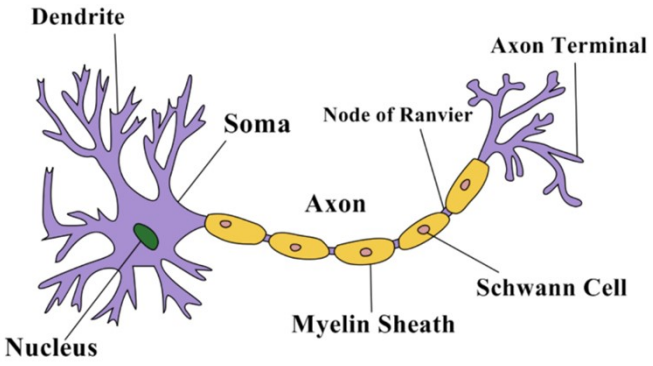

Figure 1.1: Typical neuron structure. From [5]

potential, while a bigger one generates a bigger change. Graded potentials can be excitatory (depolarizing) or inhibitory (hyperpolarizing). The amplitude of graded potentials decreases with propagation, so they travel for short distances.

An action potential is an electrical impulse generated in response to some events. It is characterized by all-or-none behaviour. This means that until the membrane voltage is under a threshold nothing happens, and when it crosses the threshold an action potential is generated. Sodium channels open, there is an increase in membrane voltage called depolarization. Then potassium channels open and sodium ones close, there is the repolarization period, when the membrane potential return to rest condition. There is also a hyperpolarization phase when membrane potential is more negative then rest condition. The hyperpolarization phase determines the refractory period, when even a supra threshold stimulus cannot generate an action potential. In Figure 1.2 we can see how the membrane potential changes during an action potential and the different phases that characterized it.

Action potentials are also called spikes; when a cell produce an action potential, we say that it fires. The number of spikes produced by the cell over a given period time is called firing rate. An action potential can be produced only after a depolarization that is bigger than the threshold, graded potential can occur due to a depolarization or due to hyperpolarization. An action potential has always the same amplitude, a bigger or longer stimulus influences only the frequency, or the number of spikes generated.

1.3 Retina structure

The retina is a stratified neural tissue approximately 0.5 mm thick in the back of the eye. It contains neuron somas arranged in three different layers, separated by two layers where synaptic connections take place. Photoreceptors are sensory neurons that responds to light stimuli whit graded potentials, they are placed

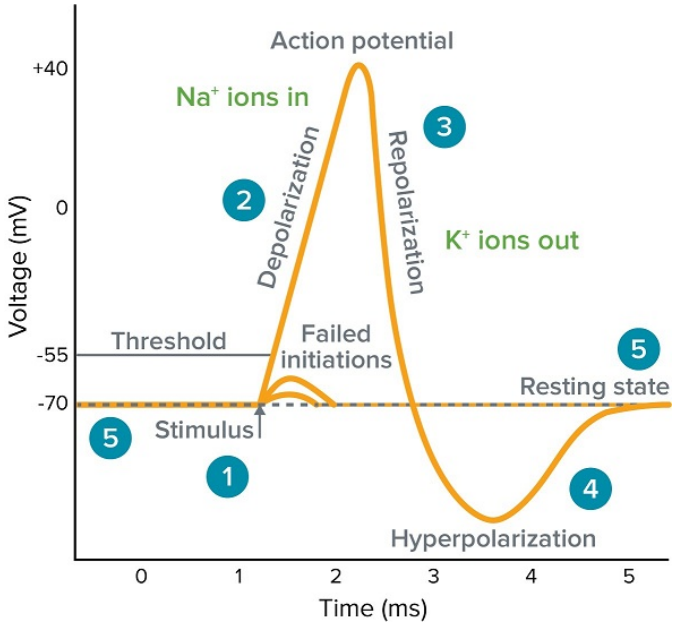

Figure 1.2: Action potential phases over the time. From [6]

in the deepest layer of the retina. Cones and rods are the two different types of photoreceptors found in human eyes. Most of the cones are concentrated in the fovea, the central region of the retina, and their density decreases in peripheral areas, while rods predominate in the periphery. Cones are responsible for colour vision and details, while rods vision is less neat but due to their higher sensibility to light, they allow night vison.

The layers that form the retina are outer nuclear layer (ONL), outer plexiform layer (OPL), inner nuclear layer (INL), inner plexiform layer (IPL), ganglion cell layer (GCL). Photoreceptors lie in the ONL and form synapses in the OPL with bipolar cells (BP). The soma of BP are in the INL, where there are also horizontal cells (HRZ) and amacrine cells (AM). In the IPL there are the synapses between BP and retinal ganglion cells (RGC), that lie in the GCL. Impulses travel from RGC to the brain trough optic nerve. Retinal structure and cell disposition within retinal layers are illustrated in Figure 1.3.

Cones and rods both hyperpolarize in response to light stimulation, whereas they are depolarized in darkness. Glutamate release increases with photoreceptor depolarization, depolarizing horizontal cells as a result. When horizontal cells depolarize, they inhibit photoreceptors as part of a negative feedback system. Additionally, cones create synapses with bipolar cells, which differ in their responses according to whether they are of the ON or OFF kind. BP off depolarize and the BP on hyperpolarize when glutamate levels rise (due to a dark stimulus). AM

A.

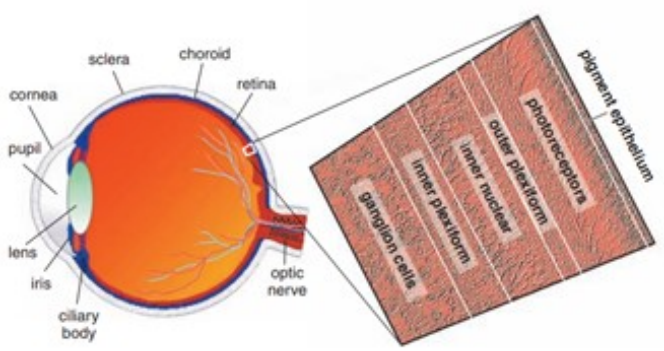

B.

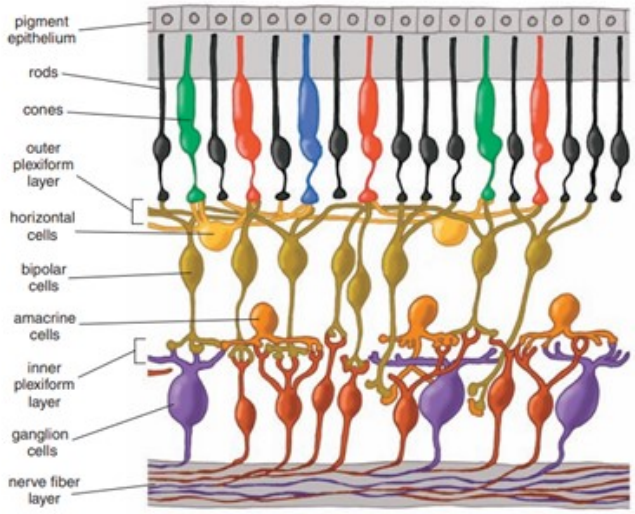

Figure 1.3: Eye and retina structure. (A) Human eye components with a focus on the layers of the retina. (B) Cells disposition within retinal layers. From [7].

and RGC form synapses with BP. In response to a light stimulation, narrow field amacrine cells inhibit RGC, while long field amacrine cells inhibit RGC off. RGC are the last group, and their axons form the optic nerve, which communicate information to the brain through the lateral geniculate nucleus. All cells in the network produce graded potentials, except for RGC, which instead produce action potentials when adequately activated.

1.4 Retinal prostheses

Electrical stimulation of the retina enables to generate a visual response in blind patients by producing bright spots called phosphenes. This approach is used to stimulate retinal ganglion cells when cones and rods are damaged following a photoreceptor degeneration like retinitis pigmentosa (RP) or age-related macular degeneration (AMD) and is based on the assumption that the rest of the retina remains intact. The number of electrodes on the implant, the stimulation techniques used, and the patient's ability to recognize different shades of grey all affect how well an image is received [8]. The implants developed are based on external image acquisition with a camera. The image is processed externally to reduce the amount of information to be transmitted to the implant. The data is transmitted wirelessly to the implant, which converts it into an electrical stimulation pattern [9].

There are three main types of retinal prosthesis based on the position of the electrode array: epiretinal, subretinal, suprachoroidal [9, 10]. Their position with respect to the retinal cells is shown in Figure 1.4.

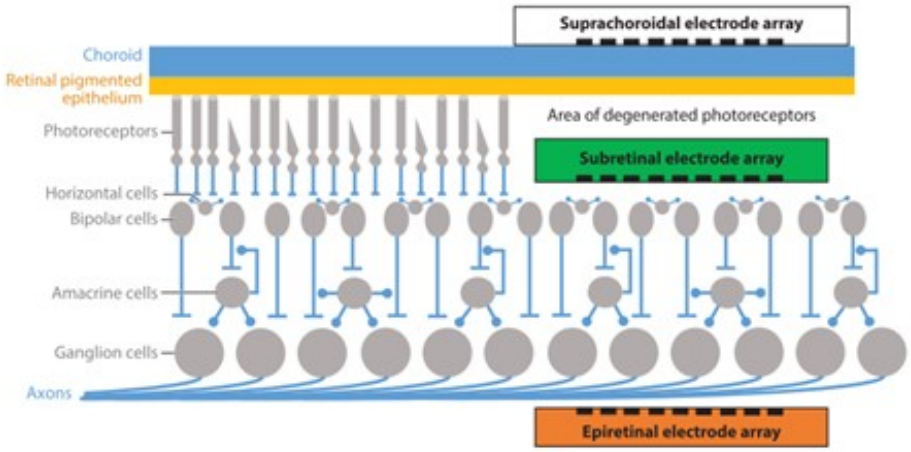

Figure 1.4: Common locations of electrode arrays in retinal prostheses. From [10].

1.4.1 Epiretinal prosthesis

For epiretinal prosthesis the implant is placed under the RGC layer, in the vitreous space. This solution has the advantage of being the closest one to the RGC, so lower currents may be applied but a more complex image processing is required to replace the retinal one. In this placement the vitreous can serve as a heat sink helping with heat dissipation from the device [11].

1.4.2 Subretinal prosthesis

In subretinal prosthesis the electrode array is placed at the photoreceptor level, between the bipolar cells and the retinal pigmented epithelium. The implant is closer to the next surviving cells in the visual pathway, bipolar cells, this allows to exploit the retinal processing. The restricted subretinal area for electronics placement and the retina near proximity to the electronics raise the risk of thermal injury to the neurons [9].

1.4.3 Suprachoroidal prosthesis

In suprachoroidal prosthesis the implant is placed between the sclera and the choroid. The advantages of this approach are that the surgery is easier and less invasive to the retina, the implant is also more stable. However, the electrodes are further from the retinal ganglion cells, so higher currents should be applied to elicit neural response. Additionally, the resolution will be limited by an increase in the receptive field of each electrode caused by current spread before the current reaches the neurons [8],[9].

1.5 Hybrid modelling

Computational models provide a better understanding of how the retina works, which is essential to improve present implants. Hybrid models (HMs) are used to model neural response to electrical stimulation. They are divided in two main steps: the solution of a volume conduction problem to compute the electrical potential generated by an electrode and the neural response to that potential [12]. HMs have been successfully used to model electrical stimulation of peripheral nerves [1], spinal cord [2], and for deep brain stimulation [3]. The results obtained in these situations lead us to think that HM can be effectively used to model retinal electrical stimulation.

When the geometry of the electrodes and of the surrounding tissues have been heavily simplified, the electric potential distribution can be computed in closed form, as will be illustrated in the Methods. For more complicated geometries and boundary conditions, analytical solutions cannot be obtained. HMs typically use FEM to compute the electric potential generated through electrical stimulation. FEM is a numerical method used for solving partial differential problems. FEM has been used to simulate retinal electrical stimulation considering vitreous, photoreceptor layer and the rest of the retina as a single layer [13].

Modelling all the layers allows to study how different position of the electrode affect result. Moreover, different retinal layers can be modified to simulate degenerations, changing tissue thickness or conductivity. For example in [14], RPE,

OPL, and ONL were removed and INL and IPL thickness were reduced to simulate retinal degeneration.

To study neuron responses to retinal electrical stimulation, many models have been proposed that detail the functioning of a single cell [15], or that consider the entire retinal network [16]. In their review, Guo and colleagues identified six main types of models that are used in modelling retinal neurons: single compartment models, morphologically realistic models, block compartment models, block-structured models of retinal function, discrete neuronal network models [17]. Here, we will consider single compartment models and morphological models.

Single compartment models (also known as point models), describe the behaviour of the single cell; they have been implemented for almost all types of neurons in the cell. These models also describe the ionic mechanisms of the cell, which are more complex than those described by the Hodgkin-Huxley model. Although these models have the benefit of being easy, they do not accurately capture all the properties of retinal neurons, necessitating the implementation of a varied ion channel distribution in each portion of the cell.

Morphological realistic models are cell models that consider the anatomy of the cell, they can include soma, dendrites, and axon. They allow to model the different distribution of ion channels in different parts of the cell and to study how different section react to stimulation. These models can be very detailed, with lots of segments. These kinds of model have been developed for almost all retinal cells, there are BP models [18], AM models [19]. RGC morphological models that have been proposed include ionic mechanism that are variations of Hodgkin-Huxley model. These models have the advantage that can be very detailed, but they also require a lot of computational time. For this reason, they cannot be easily used to simulate a high number of cells or whole populations.

Chapter 2

Methods

In the present thesis, we introduce a simulation framework to study retinal response to electrical stimulation. HM was used to model the volume conduction and the neural response to electrical potential. The implemented model consists of three main blocks: a retinal network model, a RGC morphological neuron model and a FEM model. In Figure 2.1, we show the flowchart of the whole model. The electrical potential distribution generated by the electrode current injection is computed through FEM and used as input to the retinal network model where cells of different populations are modelled as point-neurons. The network model is used to compute a synaptic current, which can be applied, together with the extracellular field due to electrode current injection, to the RGC morphological neuron model. Finally, the spiking activity of these RGC models is the information that reaches the visual cortex.

2.1 Retinal network model

The retinal network model used to estimate the synaptic current that reaches retinal ganglion cells has been implemented following the model proposed by Cottaris and Elfar [4]. They consider 9 different types of cells: cones, horizontal cells (HRZ), on bipolar cells (BPon), off bipolar cells (BPoff), on wide field amacrine cells (AMWFon), on wide field amacrine cells (AMWFoff), on narrow field amacrine cells (AMNFon), on retinal ganglion cells (RGCon) and off retinal ganglion cells (RGCoff).

The synapses implemented in the model are those between cones - HRZ, HRZ - cones, cones - BP, BP - AMWF, BPon - AMNFon, BP - RGC, AMWF - RGC, AMNFon – RGCoff. A $300 \times 300\,\mu m^2$ portion of the retina has been considered.

The cells are modelled as point neurons and are organized according to regular

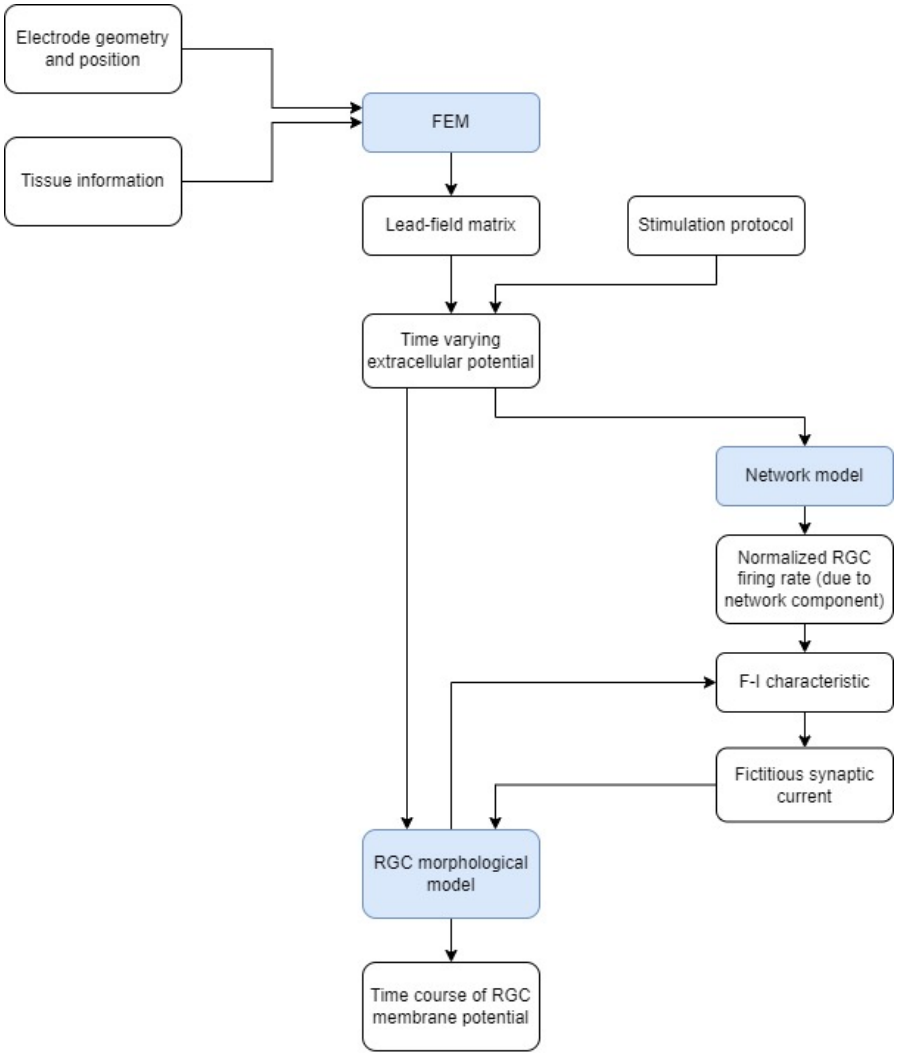

Figure 2.1: Flowchart of the model.

mosaics, with the soma x and y coordinates given by:

$$p_{i,j} = [l\ m]x \begin{bmatrix} 1 & \sqrt{3} \\ 1 & -\sqrt{3} \end{bmatrix} \lambda_j + n_{i,j} \quad l, m = 0, \pm 1, \pm 2, \ldots$$

where λ_j is a number specific for each population that defines the spacing between cells and $n_{i,j} \sim \mathrm{N}([0,0], \sigma_j)$.
Soma z coordinates are assigned between a minimum and maximum value specific for each cell population, $z_{i,j} \sim \mathrm{U}(z_{\min,j}, z_{\max,j})$.

Figure 2.2 shows the mosaics of each cell population and the $3D$ distribution of the cells in the retinal layers.

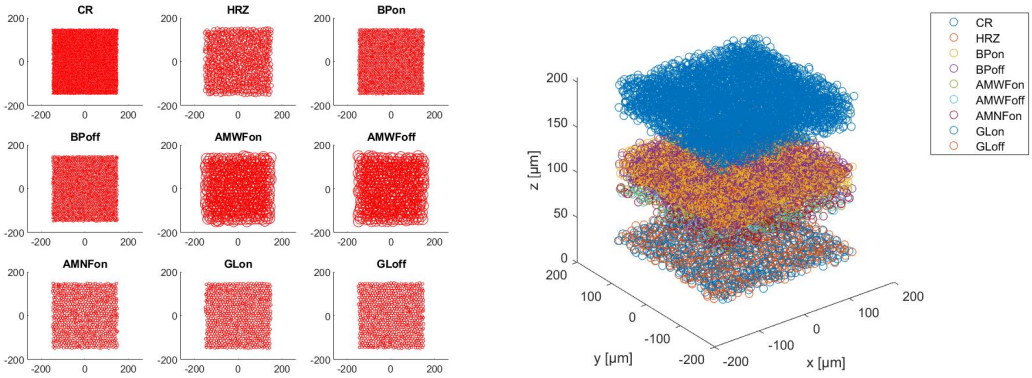

Figure 2.2: Cell spatial distribution. On the left mosaics of each population are shown, xy plane is represented. The right part of the figure shows the 3D cell distribution, cells soma are represented. Three different layers can be identified.

The membrane potential of each cell changes according to:

$$C_m \frac{dV_m}{dt} = I_{\text{leak}}\,(t) + I_{\text{extracellular}}\,(t) + \sum_{syn} I_{syn}(t)$$

where I_{leak} is the leakage current,$I_{\text{extracellular}}$ the current related to extracellular stimulation, and I_{syn} the current resulting from synaptic activation.
The leakage current is defined by:

$$I_{\text{leak}}\,(t) = G_m\,[E_{\text{rest}} - V_m(t)]$$

where G_{m} is the membrane conductance due to the presence of non-gated ion channels on the soma of the cell, E_{rest} is the rest potential and $V_{\text{m}}(t)$ is the membrane potential. This means that whenever the membrane potential is different from the rest value, a leakage current is generated that exponentially pushes the membrane potential to rest.

The activation of a specific type of synapse generates a synaptic current given by:

$$I_{syn}(t) = G_{syn}(t)\,[E_{syn} - V_m(t)]$$

where E_{syn} is the reversal potential of the synaptically-gated channel and G_{syn} is the total channel conductance, it is an integration of all the single channel conductance of the channels gated by a type of synapse. The synapse is excitatory if $E_{syn} > E_{rest}$ (the current tends to increase the membrane potential with respect to rest), while it is inhibitory if $E_{\text{syn}} < E_{\text{rest}}$ (the current tends to decrease the

membrane potential with respect to rest). In fact,

$$C_m \frac{dV_m}{dt} = I_{\text{leak}}(t) + \sum_{syn} I_{\text{syn}}(t)$$

$$C_m \frac{dV_m}{dt} = G_m \left[E_{\text{rest}} - V_m(t)\right] + G_{\text{syn}}(t) \left[E_{\text{syn}} - V_m(t)\right]$$

At infinity $V_m \to E_{\text{rest}}$

$$C_m \frac{dV_m}{dt} = G_{syn}(t) \left[E_{syn} - E_{\text{rest}}\right]$$

$$\frac{dV_m}{dt} > 0 \text{ if } E_{\text{syn}} > E_{\text{rest}}$$

G_{syn} is controlled by a presynaptic input g_{syn} weighted with respect to the distance between presynaptic and postsynaptic cells.

$$G_{syn}(t) = \frac{1}{W} \sum_p g_{syn,p}(t) \exp\left[-\frac{D(p_0, p)}{\sigma}\right]$$

$$W = \sum_p \exp\left[-\frac{D(p_0, p)}{\sigma}\right]$$

$D(p_0, p)$ is the Euclidean distance between the presynaptic and postsynaptic neuron. In this way synapses between closer cells have more weight than that between more distant ones.

g_{syn} increase or decrease monotonically between the maximum and minimum value, $g_{\max}$ and $g_{\min}$.

$$g_{syn} = \begin{cases} g_{\min} + (g_{\max} - g_{\min})\, x \left(1 - \left[1 + \exp\left(\frac{V_{\text{presynaptic}}(t - \tau_{\text{syn}}) - V_{50}}{\beta}\right)\right]^{-1}\right) \\ \text{for a monotonically increasing conductance} \\ \\ g_{\min} + (g_{\max} - g_{\min})\, x \left[1 + \exp\left(\frac{V_{\text{presynaptic}}(t - \tau_{xyn}) - V_{\text{so}}}{\beta}\right)\right]^{-1} \\ \text{for a monotonically decreasing conductance} \end{cases}$$

τ_{syn} is the delay introduced by the synapse, $V_{\text{presynaptic}}(t - \tau_{\text{syn}})$ is the delayed membrane potential of the presynaptic neuron, V_{50} and β are the values of the center operating point and the steepness of the synaptic transfer function. The synapses can be excitatory or inhibitory, increasing or decreasing. All the parameters used for the model are listed in Table 2.1, except for the ones used to model synapses, that are listed in Table 2.2.

Figure 2.3 shows how g_{syn} changes with V_m.

The interaction between the light stimulus and cone reaction in case of visual stimulation is given by:

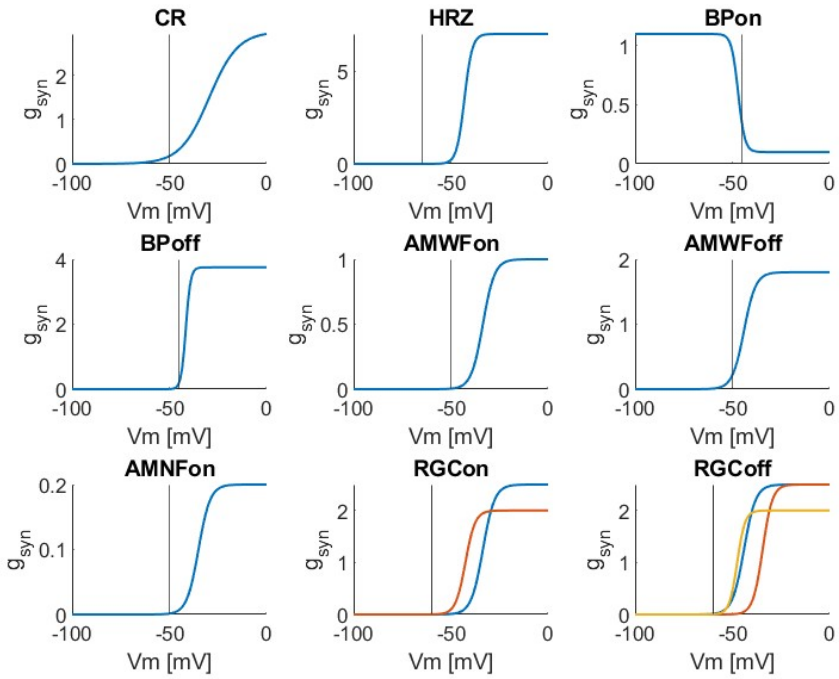

Figure 2.3: Synaptic conductance. The figure shows how g_{syn} changes with a membrane potential increase.

$$G_{\text{light}}(t) = g_{\min} + (g_{\max} - g_{\min})\left[L_{\max} - L\left(t - \tau_{photo}\right)\right]$$

where L is the light intensity (between 0 and 1) and $L_{\max}$ is the maximum light intensity (=1).

The extracellular current is given by

$$I_{\text{extracellular}} = \frac{1}{2} G_m \Delta V_e(t)$$

ΔV_e is the potential drop due to the extracellular stimulation. In this case the membrane conductance is halfed because the extracellular current crosses the membrane twice, when it enters and when it exits, so the resistance is doubled.

The activation function is given by:

$$\Delta V_e = \left|V_e\left(p_0 + p\right) - V_e\left(p_0 - p\right)\right|$$

$$\text{With } D\left(p, p_0\right) = \frac{d_{\text{soma}}}{2}$$

where p_0 is the position of the soma center and p is a point at radius distance from the center. The activation function is obtained by mediating the voltage value at diametrically opposite points in x, y, z direction.
The equation:

$$C_m \frac{dV_m}{dt} = I_{\text{leak}}(t) + I_{\text{extracellular}}(t) + \sum_{syn} I_{syn}(t)$$

leads to:

$$\tau_m \frac{dV_m}{dt} = -V_m + V_s$$

where:

$$V_s = \frac{G_m \left(E_{\text{rest}} + \frac{1}{2}\Delta V_e\right) + \sum_{syn} G_{syn} E_{\text{syn}}}{G_m + \sum_{syn} G_{syn}}$$

$$\tau_m = \frac{C_m}{G_m + \sum_{syn} G_{syn}(t)}$$

The membrane potential of RGCs is used to compute a normalized firing rate:

$$S(t) = \frac{[\delta V(t)]^n}{[\delta V(t)]^n + [\delta V_0]^n}$$

where:

$$\delta V(t) = \max[0, V_m(t) - E_T]$$

$$n = 2 + [0.1\delta V(t)]^2$$

S is a sigmoid function with steepness defined by n, δV_0 is the value of $\delta V(t)$ at which we have a normalized firing rate of 0.5, and it is set to 5 mV.

The sigmoid curves to obtain the normalized firing rate from membrane voltage for RGCoff and RGCon are shown in Figure 2.4

The voltage due to extracellular stimulation in a specific point is obtained considering the potential generated by a disc electrode in a semi-infinite homogeneous medium with a return electrode at infinity:

$$V_e(x, y, z) = \frac{2V_0}{\pi} \arcsin\left[\frac{2\alpha}{\sqrt{(r+\alpha)^2 + d^2} + \sqrt{(r-\alpha)^2 + d^2}}\right].$$

$$r = \sqrt{(x - x_{\text{electrode}})^2 + (y - y_{\text{electrode}})^2}$$

$$d = z - z_{\text{electrode}}$$

$$V_0 = I_{\text{electrode}} R_{\text{tissue}}$$

x_{el}, y_{el}, z_{el} are the coordinates of the centre of the electrode, α the electrode diameter lelectrode is the current injected and R_{tiss} is the resistive impedance of the retina.

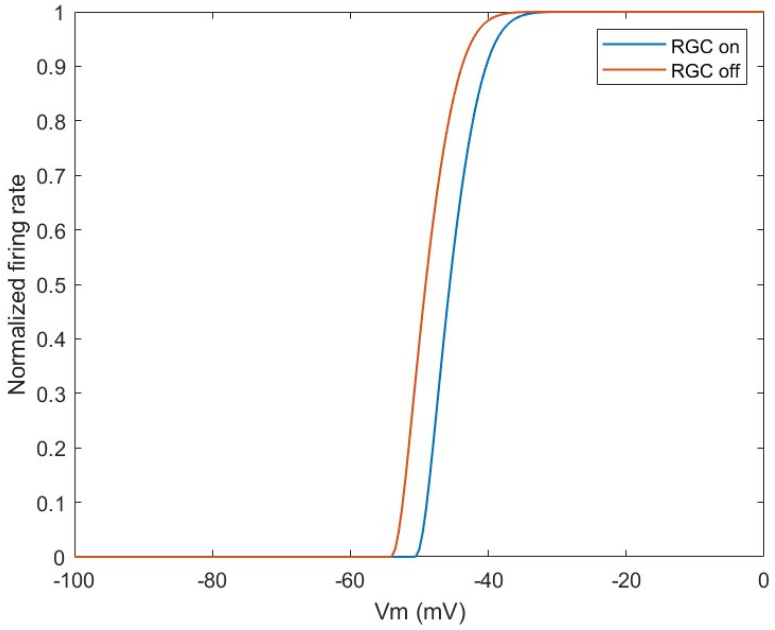

Figure 2.4: Sigmoid function to obtain RGC on and off normalized firing rate according to $V_{\mathbf{m}}$. When membrane potential is 5 mV over E_{T}, the normalized firing rate is 0.5.

Table 2.1: Values for cells position of different cell types and cells membrane characteristics Lambda sigma zmin and zmax are in µm, Cm is in pF, Gm is in nS, tau is in ms, Erest and ET are in mV, n refers to the number of cells in the mosaic.

	CR	HRZ	BPon	BPoff	AMWFon	AMWFoff	AMNFon	RGCon	RGCoff
λ	2.5	7.0	3.85	3.85	8.0	8.0	6.0	6.0	6.0
σ	2.5	10.5	3.85	3.85	24.0	24.0	6.0	6.0	6.0
z_{min}	170	100	100	100	80	80	80	25	25
z_{max}	205	128	128	128	101	101	101	39	39
n	4105	537	1741	1741	391	391	721	721	721
C_{m}	80	210	50	50	50	50	50	50	50
G_{m}	4.0	2.5	2.0	2.0	2.0	2.0	2.0	2.0	2.0
τ_{rest}	20	84	25	25	25	25	25	25	25
E_{rest}	-50.0	-65.0	-45.0	-45.0	-50.0	-50.0	-50.0	-60.0	-60.0
E_{T}	-	-	-	-	-	-	-	-50.6	-54.1

Table 2.2: Parameters used for synaptic connections. Esyn, V50 Beta are in mV, gmin and gmax in nS. Type 'D' and 'I' refer to a decreasing or increasing conductance.

	Esyn	gmin	gmax	V_{50}	β	Type
Light-CR	-8.0	0.0	0.9	-	-	D
CR-HRZ	0.0	0.0	7.0	-43.0	2.0	I
HRZ-CR	-67	0.0	3.0	-29.5	7.4	I
CR-BPon	0.0	0.1	1.1	-47.0	1.7	D
CR-BPoff	0.0	0.0	3.75	-41.5	1.2	I
BPon-AMWFon	0.0	0.0	1.0	-33.5	3.0	I
BPon-AMNFon	0.0	0.0	0.2	-35.0	3.0	I
BPoff-AMWFoff	0.0	0.0	1.8	-44.0	3.0	I
AMWFon- RGCon	-70	0.0	2.0	-42.5	2.5	I
WFAMoff-RGCoff	-70	0.0	2.5	-34.4	2.5	I
AMNFon-RGCoff	-80	0	2.0	-47.5	2.0	I
BPon-RGCon	0.0	0.0	2.5	-33.5	3.0	I
BPoff-RGCoff	0.0	0.0	2.5	-44.0	3.0	I

2.1.1 Subsampling and surface increase

The model implemented had a $300 \times 300\,\mu\text{m}^2$ surface, which represents only a small portion of the retina. A bigger surface should be considered, but this involves a considerable increase of computational time. To try to reduce the computational time, a subsampling of the number of cells present in each mosaic was carried out, maintaining the regular structure of the lattice. Figure 2.5 shows the mosaics with total number of cells, with a 50% subsampling and with only 20% of cells of original populations. The dimensions of the retina are doubled and tripled, also with subsampling.

2.2 RGC model

In the model proposed by Cottaris and Elfar, RGCs produce a graduated potential, while it is not considered the ionic-channels dynamic that produce action potentials. The most known model the describes cell dynamics is Hodgkin-Huxley model, but it is not adequate to describe the more complex mechanism of RGCs. A lot of models have been proposed, starting from Fohlmeister-Coleman-Miller (FCM) model [20, 21, 22].

The ionic mechanism used in our RGCs model follows FCM model [20]. As a first step, a punctiform model has been implemented, then the ionic mechanism

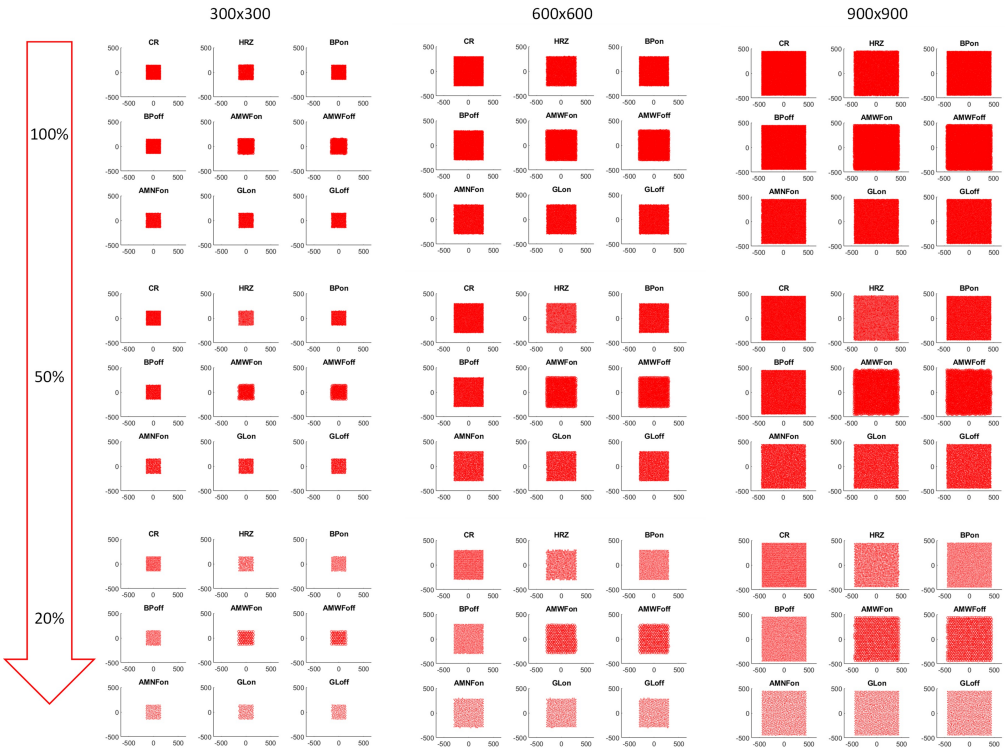

Figure 2.5: Cell mosaics with subsampling and surface increase. The first column of the figure shows cell mosaics for a $300 \times 300\,\mu m^2$ surface, in the second column the dimensions are $600 \times 600\,\mu m^2$, while in the third column $900 \times 900\,\mu m^2$. The first row of the figure shows cell mosaics with complete populations, the second row is applied a subsampling of 50% of the cells, the last row shows mosaics made of only 20% of original population.

has been inserted into a morphological model that represents the soma and the axon of the cell.

In FCM model the voltage membrane is controlled by five ionic currents $\left(\mathrm{Na}^{2+}, \mathrm{Ca}^{2+}\right.$ and three types of K^{+}currents), a leakage current and the current resulting from electrical stimulation.

$$C_m \frac{dV}{dt} + \overline{g_{Na}} m^3 h \left(V - V_{Na}\right) + \overline{g_{Ca}} c^3 \left(V - V_{Ca}\right)$$
$$+ \left(\overline{g_K} n^4 + \overline{g_{K,A}} a^3 h_A + g_{K,Ca}\right) \left(V - V_K\right) + \overline{g_L} \left(V - V_L\right) = I_{stim}$$

V_{Ca}, V_{Na} and V_K are the equilibrium potentials of calcium, sodium, and potassium. V_{Na} and V_K are assumed constant, while only V_{Ca} changes according to Nernst equation.

$$V_{Ca} = \frac{RT}{2F} \ln \left\{ \frac{\left[\mathrm{Ca}^{2+}\right]_e}{\left[\mathrm{Ca}^{2+}\right]_i (t)} \right\}$$

Four of the ionic currents are voltage gated, while $g_{K,Ca}$ is gated by the intracellular calcium concentration $\left[\mathrm{Ca}^{2+}\right]_i$

$$g_{K,Ca} = \overline{g_{K,Ca}} \frac{\left(\left[\mathrm{Ca}^{2+}\right]_i / \left(\mathrm{Ca}^{2+}\right)_{\mathrm{diss}}\right)^2}{1 + \left(\left[\mathrm{Ca}^{2+}\right]_i / \left(\mathrm{Ca}^{2+}\right)_{\mathrm{diss}}\right)^2}$$

where $\left(\mathrm{Ca}^{2+}\right)_{\mathrm{diss}}$ is the calcium dissociation constant.
$\left[\mathrm{Ca}^{2+}\right]_i$ changes over the time according to:

$$\frac{d\left[\mathrm{Ca}^{2+}\right]_i}{dt} = \frac{-3I_{Ca}}{2Fr} - \frac{\left(\left[\mathrm{Ca}^{2+}\right]_i - \left[\mathrm{Ca}^{2+}\right]_{\mathrm{res}}\right)}{\tau_{Ca}}$$

Where $\left[\mathrm{Ca}^{2+}\right]_{\mathrm{res}}$ is the residual intracellular calcium concentration and τ_{Ca} calcium removal time constant.

m, h, c, n, a, h_A are the state variables of voltage-gated channels, they follow the first order kinetic equation described by Hodgkin-Huxley:

$$\frac{dx}{dt} = -\left(\alpha_x + \beta_x\right) x + \alpha_x$$

Where x indicates a generic state variable.

State variables depends on both voltage and time, $x(V, t)$ represents the proportion of open channels at time t and voltage V. Rate constants formulation are listed in Table 2.4. To determine initial values of state variables, the equation system has been resolved initializing them at random values. The value of state variables at infinity corresponds to the rest value, they are listed in Table 2.3

Table 2.3: Initial values for RGC model. Initial values for state variables, membrane potential and intracellular calcium concentration.

$m = 0.0182$	$A = 0.0466$
$h = 0.9286$	$h_{\mathrm{A}} = 0.409$
$c = 0.0019$	$V_{\mathrm{m}} = -65\,mV$
$n = 0.0843$	$\left[\mathrm{Ca}^{2+}\right]_{\mathrm{i}} = 0.00015\,(mM)$

Table 2.4: Rate constants equations.

$\alpha_m = \frac{-0.6(V+30)}{e^{-0.1(V+30)}-1}$	$\beta_m = 20e^{-(V+55)/18}$
$\alpha_h = 0.4e^{-(V+50)/20}$	$\beta_h = \frac{6}{e^{-0.1(V+20)}+1}$
$\alpha_c = \frac{-0.3(V+13)}{e^{-0.1(V+13)}-1}$	$\beta_c = 10e^{-(V+38)/18}$
$\alpha_n = \frac{-0.02(V+40)}{e^{-0.1(V+40)}-1}$	$\beta_n = 0.4e^{-(V+50)/80}$
$\alpha_A = \frac{-0.006(V+90)}{e^{-0.1(V+90)}-1}$	$\beta_A = 0.1e^{-(V+30)/10}$
$\alpha_{hA} = 0.04e^{-(V+70)/20}$	$\beta_{hA} = \frac{0.6}{e^{-0.1(V+40)}+1}$

Table 2.5: Values for RGC point model

$V_K = -75\text{mV}$	$\overline{g_{Na}} = 50\,[\text{mS/cm}^2]$	$\left[\text{Ca}^{2+}\right]_{\text{res}} = 0{,}001\text{mM}$
$V_{Na} = 35\text{mV}$	$\overline{g_{Ca}} = 2.2\,[\text{mS/cm}^2]$	$\left(\text{Ca}^{2+}\right)_{\text{diss}} = 0.001\text{mM}$
$V_L = -65\text{mV}$	$\overline{g_K} = 12\,[\text{mSS/cm}^2]$	$[\text{Ca}^{2+}]_e = 1.8\text{mM}$
$C = 1\,[\mu\text{F/cm}^2]$	$\overline{g_{K,A}} = 36\,[\text{mS/cm}^2]$	$\tau_{Ca} = 1.5$ ms
$R = 8.314[\ \text{J/K, mol}]$	$\overline{g_{K,Ca}} = 0.05\left[\text{mS}^2/\text{cm}^2\right]$	$T = 22°\text{C}$
$\text{F} = 96.485[\text{C/mmol}]$	$\overline{g_L} = 0.05\,[\text{mS/cm}^2]$	$r = 12.5\mu\text{m}$

All the other values used for the point model are listed in Table 2.5.

The FCM mechanism was then inserted into a morphological model of a RGC consisting of soma and axon, implemented with Neuron. In this way, it is possible to define different geometries for the soma and axon and assign them different conductivity values, representing the different distribution of ion channels on the neuron sections. The model consists of two sections, soma and axon, each of them is divided into more segments. In a compartment model is possible to simulate extracellular stimulation, while with the punctiform model it is possible to simulate only the intracellular one. The soma has diameter and length of $30\,\mu m$, while the axon had $1\,\mu m$ diameter and is long $2\,mm$. Values used for channel densities in the soma and in the axon are taken from Greenberg [23] and are listed in Table 2.6.

Intracellular stimulation reflects the effects of synaptic current. First the

Table 2.6: Channel conductances used in the RGC morphological model. From [23]

G (mS/cm2)	Soma	Axon
gNa	70	150
gCa	1.5	1.5
gK	18	18
gK,A	54	54
gK,Ca	0.065	0.065

frequency-intensity curve is obtained, modelling $I_{\text{intracellular}}$ as a constant value. From the frequency-intensity curve it is possible to obtain the current intensity required to produce a given firing rate. The maximum firing rate value of that curve corresponds to level 1 of normalized firing rate, while all other firing rates are computed as a percentage of the maximum value. This firing rate is then converted into a synaptic current.

The firing rate used to compute the synaptic current does not consider the contribution of extracellular stimulation, so V_s used for RGC in retinal network model becomes

$$V_s = \frac{G_m E_{\text{rest}} + \sum_{\text{syn}} G_{\text{syn}} E_{\text{syn}}}{G_m + \sum_{\text{syn}} G_{syn}}$$

The extracellular stimulation has been first modelled on the hypothesis of an infinite, isotropic and homogeneous medium.

$$V(x, y, z) = \frac{I}{4\pi\sigma d}$$

Where d is the distance from the electrode.

In the final model the potential due to extracellular stimulation is computed trough FEM.

2.3 FEM

To solve a system of partial differential equations with complicated geometries and boundary conditions FEM is used [12].

The layers considered in the model are vitreous, ganglion cell layer, inner plexiform layer, inner nuclear layer, outer plexiform layer, outer nuclear layer, subretinal space, retinal pigment epithelium, choroid, sclera. The conductivity values used are taken from [14], while the thickness values are adapted to be coherent with network model cells position. The retina surface is $1 \times 1\, mm^2$, all

the other values used are listed in Table 2.7. A disc electrode with radius $50\,\mu m$ and height $10\,\mu m$ has been used for current injection. The electrode was placed at different depths to simulate epiretinal, subretinal and suprachoroidal stimulation, the values of z coordinate are listed in Table 2.8 . The return electrode has been modelled as a disc electrode of same size of the stimulation one and it was placed in the sclera layer at $z = 0.676\,mm$ and set to ground. The electrode is in a layer representing electrode body, with $\sigma = 10^{-10}\,S/m$ and thickness $30\,\mu m$. The external layer was modelled as saline with $\sigma = 2\,S/m$ and it was set to ground.

Table 2.7: Layer conductivity and thickness.

Layer	Conductivity (S/m)	Thickness (μm)
Vitreous	1.28	400
Ganglion Cell	0.02262	20
Inner Plexiform	0.03717	35
Inner Nuclear	0.01277	49
Outer Plexiform	0.019	16
Outer Nuclear	0.01244	31
Subretinal Space	0.04831	40
Retinal Pigment Epithelium	0.0147	20
Choroid	0.030874	200
Sclera	0.019	240

The FEM has been computed with an input current of $1\,\mu A$. In this way we obtain the coefficient of the lead field matrix, then to compute the potential due to other currents it is sufficient to multiply these coefficients for the current value.

To find the position where compute the FEM it is necessary to translate from network model reference system to fem reference system. The FEM is computed into the six positions at diametrically opposed points used for the network model. The FEM is also used to compute the electric potential to apply to RGC morphological model, in the positions of the nodes of soma and axon.

Table 2.8: Electrode position for different implants.

Implant	Z (mm)
Epiretinal	0.045
Subretinal	0.129
Suprachoroidal	0.436

In Figure 2.6 it is shown a 3D representation of the FEM geometry and the corresponding layers.

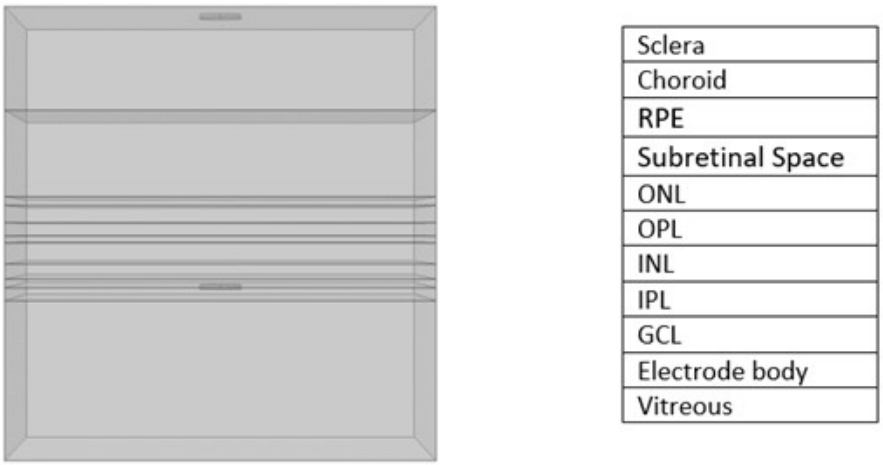

Figure 2.6: Retinal layers of the FEM.

Chapter 3

Results

3.1 Retinal network model

3.1.1 Visual stimulation

The network model has been tested for both visual and electrical stimulation. For the visual stimulation three different situations have been tested: a dark stimulus, a bright one, and a stimulus with dark and bright parts together. The dark and bright stimuli consisted of a black and a white square respectively of dimensions $50 \times 50\,\mu m^2$. The last visual stimulus consisted of a checkerboard, as showed in the Figure 3.3. The stimulus was applied for $30\,ms$, the intensity level in absence of the stimulus was set at 0.5.

Figure 3.1 shows the output of visual stimulation with a dark stimulus. Cones, HRZs, and off pathway cells depolarize, while on pathway cells hyperpolarize. This reflects in an increase of RGCoff firing rate, while RGCon activity is not present. With a bright stimulus the cells behave in the opposite way, as shown in Figure 3.2.

In the case of checkerboard stimulation showed in Figure 3.3, some cells between the same population depolarize and others hyperpolarize, based on the portion of the stimulus they receive.

3.1.2 Electrical stimulation

The electrical stimulation was provided by an electrode with $100\,\mu m$ diameter, situated $2\,\mu m$ under the RGC layer. The current impulse had $500\,\mu A$ amplitude and was applied for $30\,ms$. Electrical stimulation is conducted in absence of photoreceptor, to simulate a degenerated retina. The potential in each point is

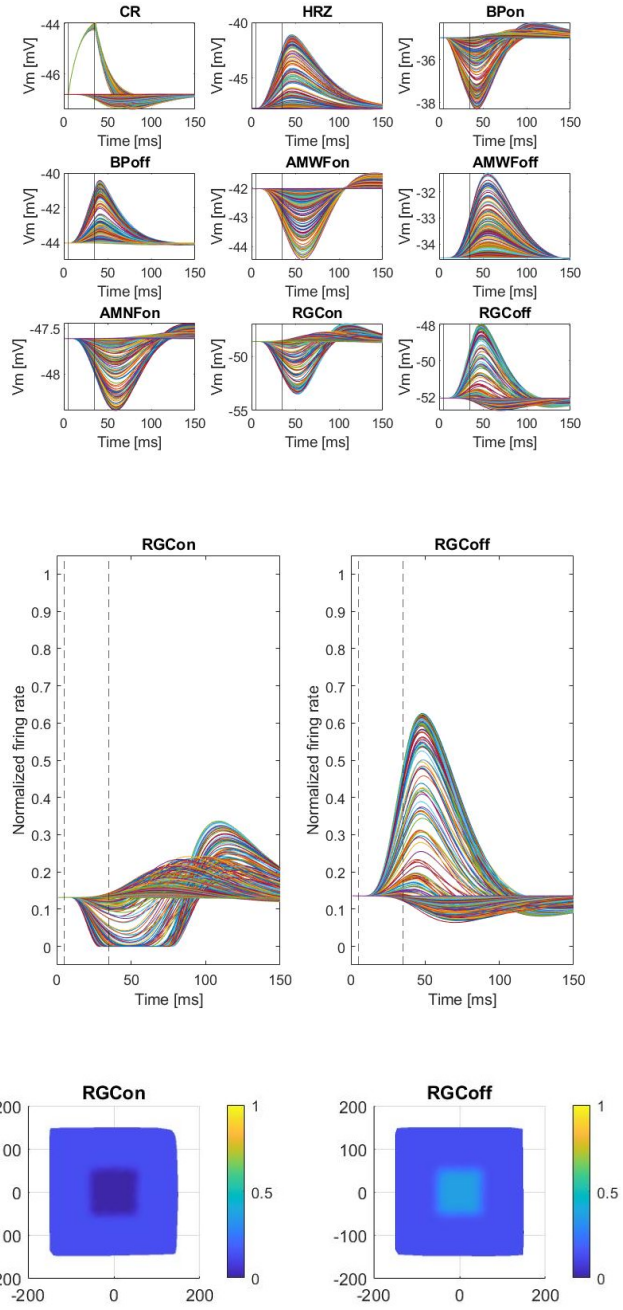

Figure 3.1: Output of visual stimulation with a dark stimulus. The upper plot shows membrane potential during stimulation for each cell population. Dotted lines indicate stimulus duration. The middle plot shows the normalized firing rates for RGCon and RGCoff. The lower plot shows spatial activation of RGCon and RGCoff cells at time 30 ms considering normalized firing rate values.

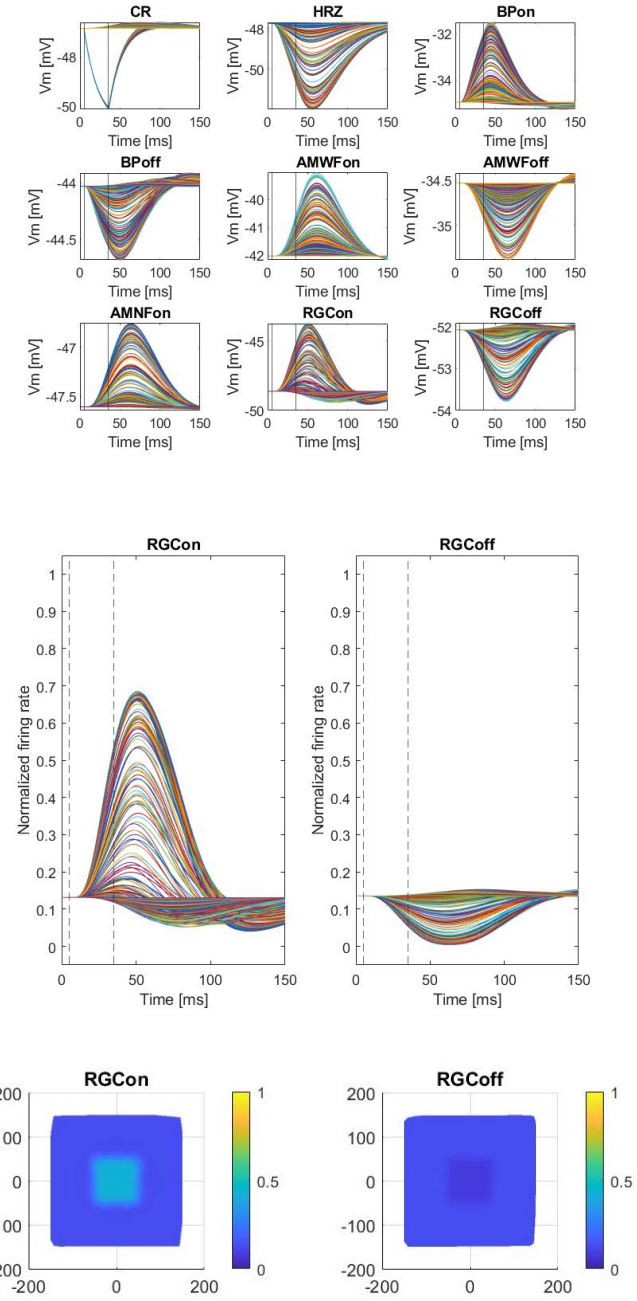

Figure 3.2: Output of visual stimulation with a bright stimulus. The upper plot shows membrane potential during stimulation for each cell population. Dotted lines indicate stimulus duration. The middle plot shows ormalized firing rates for RGCon and RGCoff. The lower plot shows spatial activation of RGCon and RGCoff cells at time 30 ms considering normalized firing rate values.

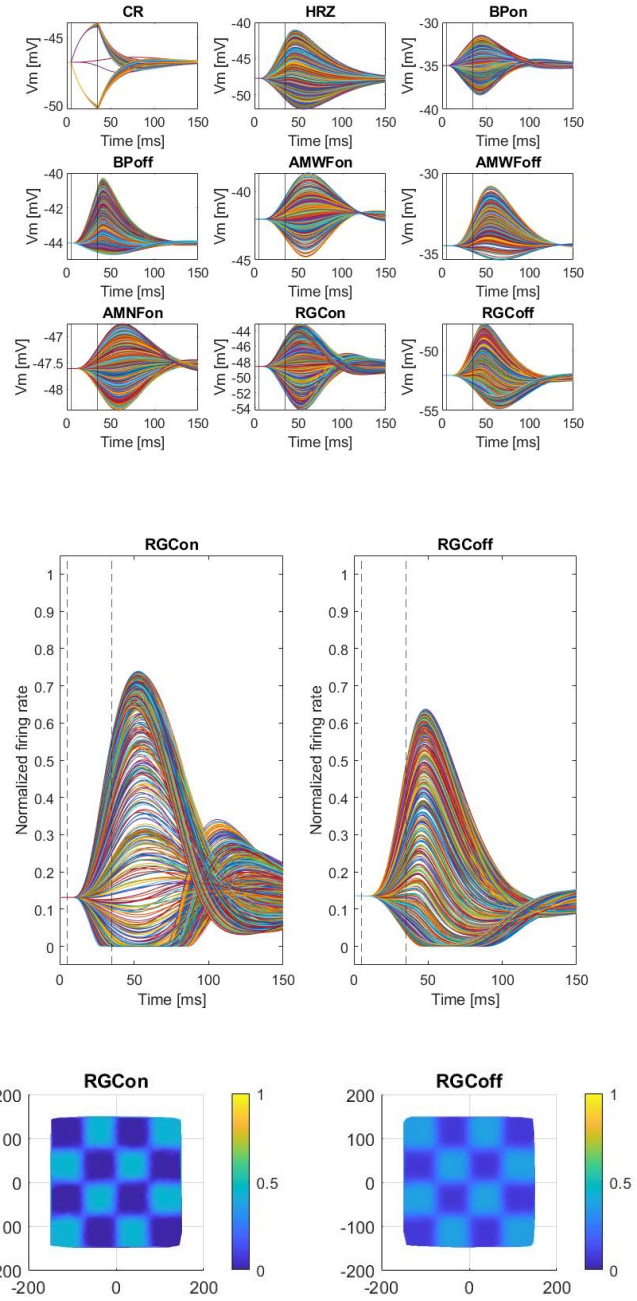

Figure 3.3: Output of visual stimulation with a checkerboard stimulus. The upper plot shows membrane potential during stimulation for each cell population. Dotted lines indicate stimulus duration. The middle plot shows the normalized firing rates for RGCon and RGCoff. The lower plot shows spatial activation of RGCon and RGCoff cells at time 30 ms considering normalized firing rate values.

compute using:

$$V_e(x,y,z) = \frac{2V_0}{\pi} \arcsin\left[\frac{2\alpha}{\sqrt{(r+\alpha)^2+d^2}+\sqrt{(r-\alpha)^2+d^2}}\right]$$

Stimulus characteristics, membrane voltage of each population, RGCon-RGCoff normalized firing rates and spatial activation are shown in Figure 3.4. All types of population depolarize after an electrical stimulus, so both on and off pathways are activated at the same time. The normalized firing rate of RGCon reaches the saturation level, this phenomenon does not happen for visual stimulation.

3.1.3 Subsampling

To reduce computational time, the number of neurons for each population has been reduced, maintaining the regular structure of the lattice. Figure 3.5 shows membrane voltage obtained with a visual stimulus for the complete population and the one with 50% of neurons and the maximum difference between the two cases in terms of membrane voltage and normalized firing rate. Every cell of the subsampled population has been compared with the one in the same position of the complete population. The overall trend is the same for both cases, the maximum error in terms of membrane potential is around $0.8\,mV$ and in terms of normalized firing rate is 0.1. Computational time was measured for complete population and subsampled ones, as shown in Figure 3.6. The same figure also shows how computational time increase with a surface increase.

3.2 RGC model

RGC model has been implemented first as a point-model, then FCM mechanism has been inserted into a morphological model.

3.2.1 Point model

The response of the point model to intracellular stimulation is shown in Figure 3.7. The firing rate of the cell increase with the current until a saturation point and then is suppressed. The point model does not allow to study differential excitability in different locations of a cell due to extracellular stimulation.

Time course of RGC membrane potential is obtained with current injection of 1, 1.5, 2, 2.5 $\mu A/cm^2$ (that for a soma of diameter 25 μm corresponds to 20, 30, 40, $50\,pA$). With a $20\,pA$ stimulation current the cell is not activated, while applying higher currents the cell increases its spiking activity. The current was applied for $400\,ms$.

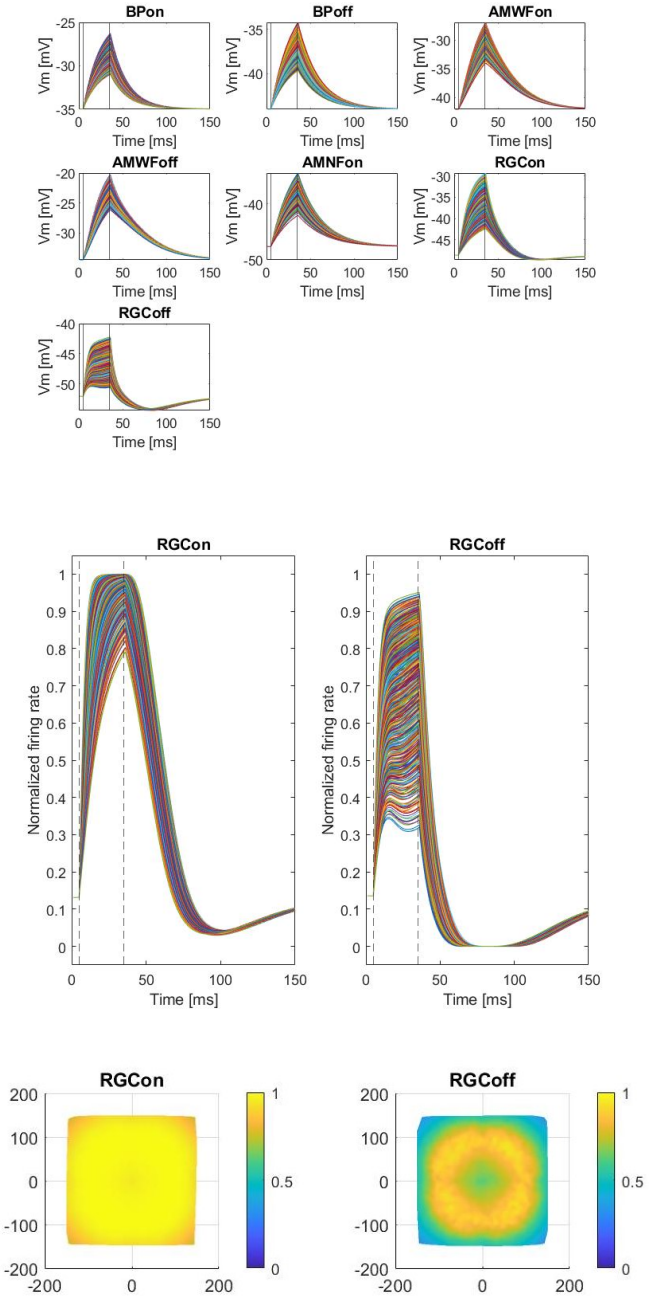

Figure 3.4: Output of electric stimulation with 500 µA current. The upper plot shows membrane potential during electrical stimulation for each cell population. Dotted lines indicate stimulus duration. The middle plot shows the normalized firing rates for RGCon and RGCoff. The lower plot shows spatial activation of RGCon and RGCoff cells at time 30 ms considering normalized firing rate values.

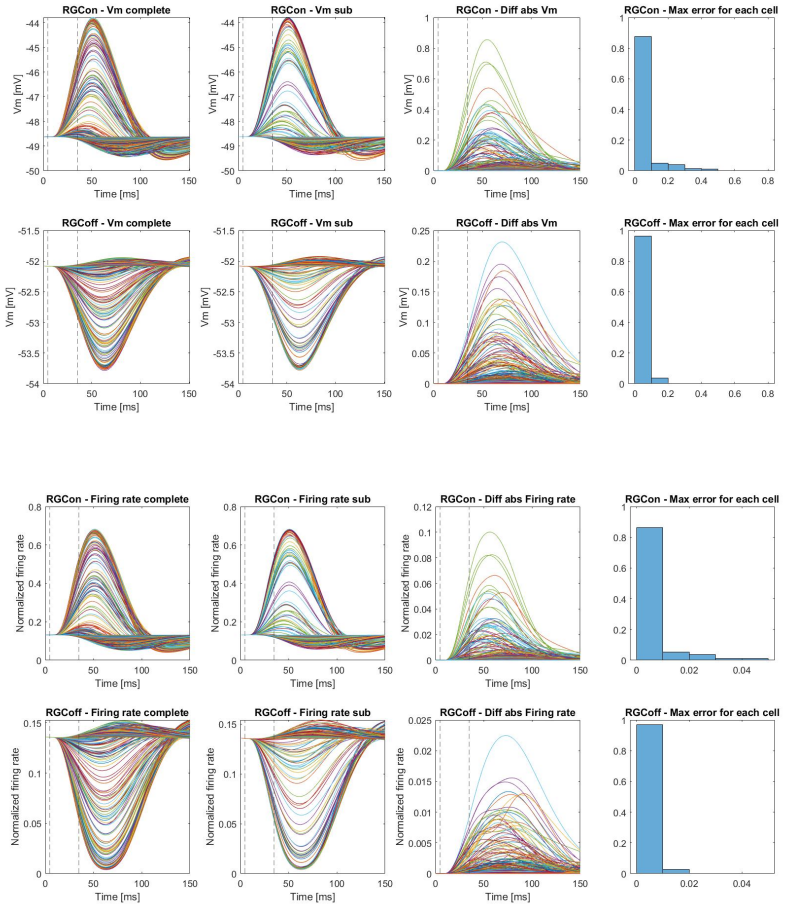

Figure 3.5: Difference between complete population and subsampled population (50%) **after a bright visual stimulus.** (Upper panel) The figure shows membrane potential of complete population and subsampled population over the time, the absolute difference of those potential for cell in the same position of the mosaics, and the histogram of maximum error committed for each cell. The first row shows results for RGCon, while the second one for RGCoff. (Lower panel) The figure follows the same format of upper panel, but shows results in term of normalized firing rate.

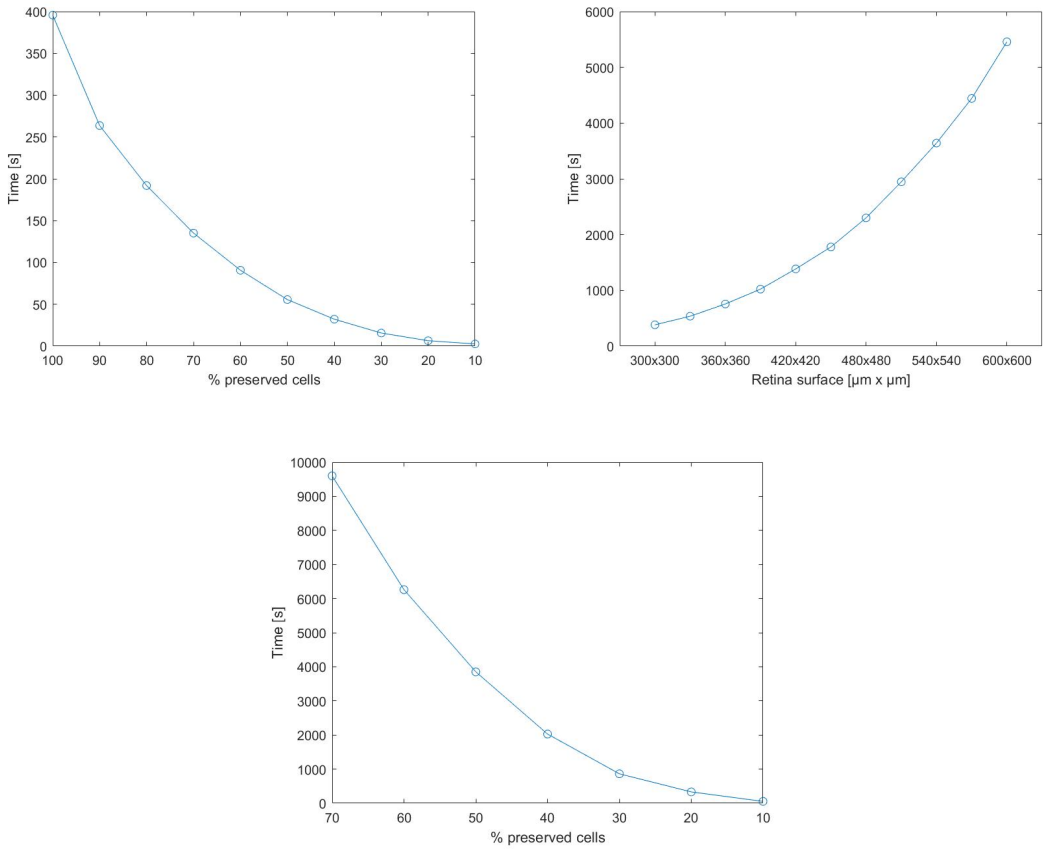

Figure 3.6: Computational time. The upper left plot shows the computational time with the subsampling the number of neurons. The upper right plot shows the computational time increasing the retina surface. The lower plot shows the computational time with a retina $900 \times 900 \mu m^2$ subsampling the number of neurons.

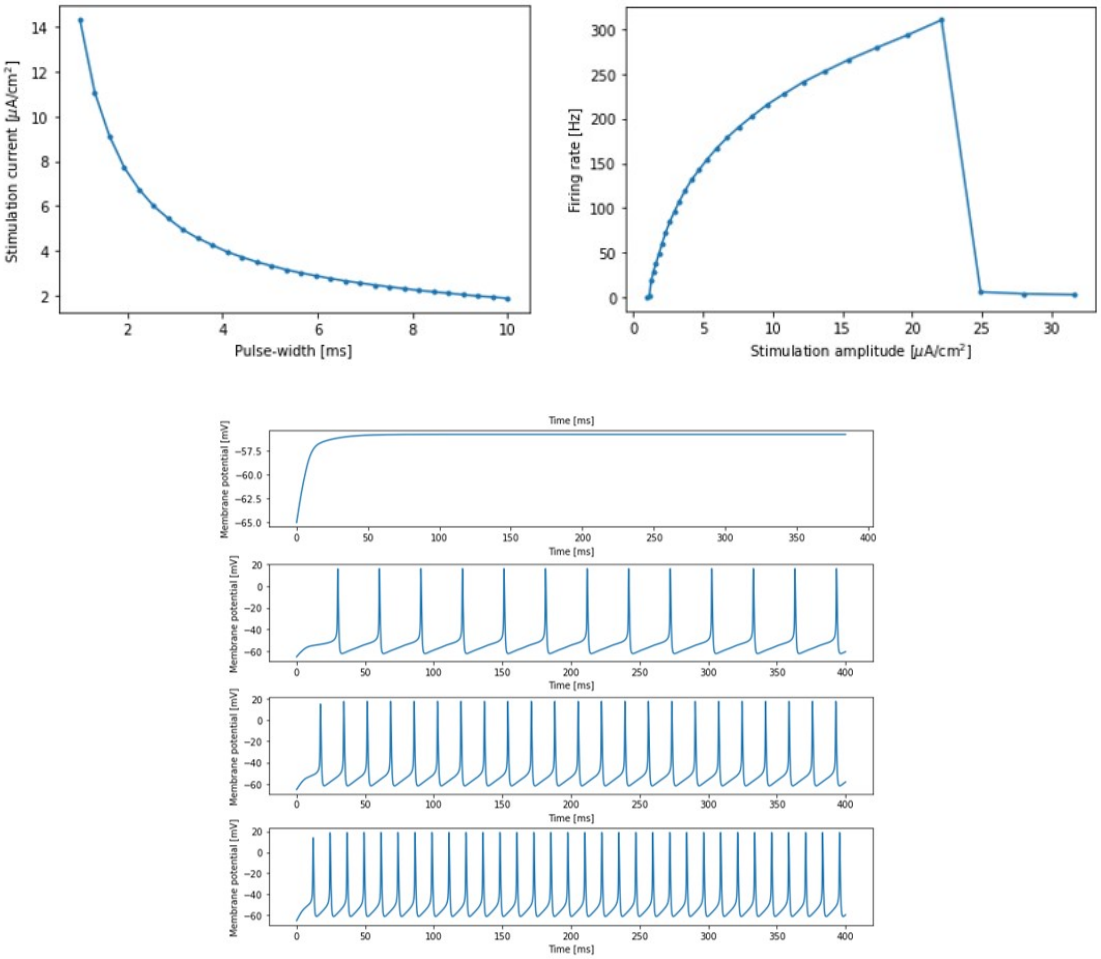

Figure 3.7: Point FCM model characterization. The upper left plot shows strength-duration curve. It shows the current required to stimulate a cell as the pulse duration changes. The upper right plot shows frequency-intensity curve. The firing rate is the spike frequency in the stimulation time. The lower panel shows cell response to increasing stimulation current.

3.2.2 Morphological model

Figure 3.8 shows the morphological RGC model response to intracellular stimulation and to the combination of intracellular and extracellular stimulation. By increasing extracellular current there is an increase also in the firing rate, this means that it is possible to modulate smoothly the RGCs firing rate applying different stimulation currents. The potential due to extracellular potential has been computed using

$$V(x, y, z) = \frac{I}{4\pi\sigma d}$$

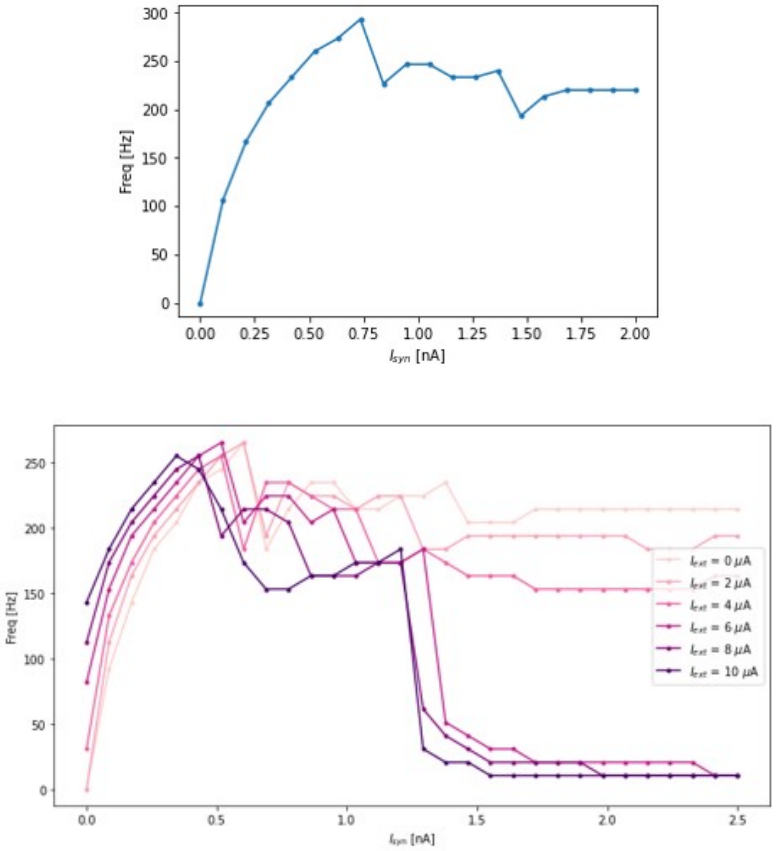

Figure 3.8: Morphological FCM model characterization. The upper plot shows frequency-intensity curve obtained with intracellular stimulation. The lower plot shows frequency-intensity curve obtained with the combination of intracellular and extracellular stimulation, considering increasing values of extracellular current.

Figure 3.9 shows cell response at different level of stimulation, when the electrode

is placed in different positions of the cell. The recording node is fixed at the end of the axon. When the current is zero the whole cell is in rest condition, then a spiking activity can be observed in the axon at lower currents when the soma is still not activated. Increasing the current also the soma is activated.

RGC morphological model also predict the production of elongated phosphenes, as shown in Figure 3.10. The electrode was placed in the centre of a regular cell grid the potential generated by a current injection of 5 $\mu A/cm^2$ activated not only the cells closer to the electrode, but also the ones whose axons passed close to it.

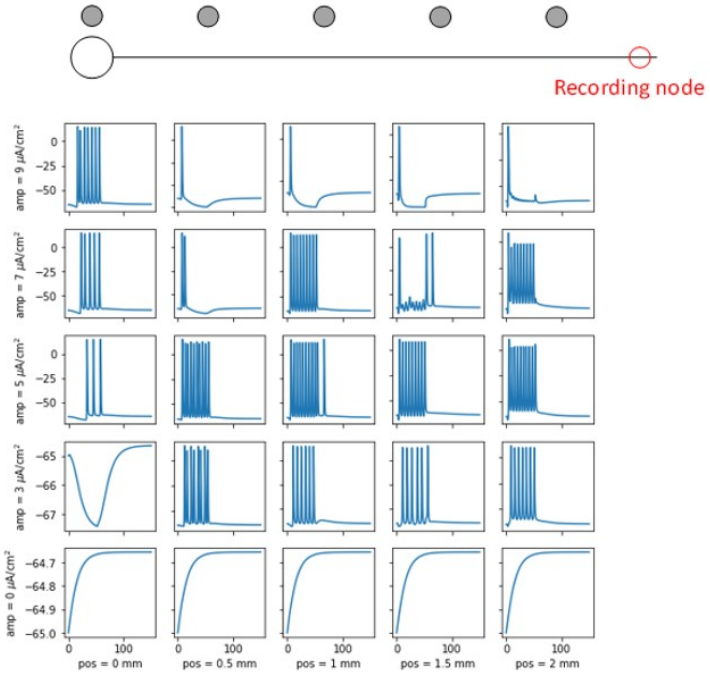

Figure 3.9: Spiking activity changing electrode position, with increasing currents. The recording node is placed at the end of the axon.

3.3 FEM

The electrical potential generated by the electrode current injection was then computed through FEM. Figure 3.11 shows electric potentials generated with a 1 μAcurrent in three different situations: epiretinal, subretinal and suprachoroidal stimulation. The potential that reaches RGC layer is higher in epiretinal stimulation because the implant is closer to RGC.

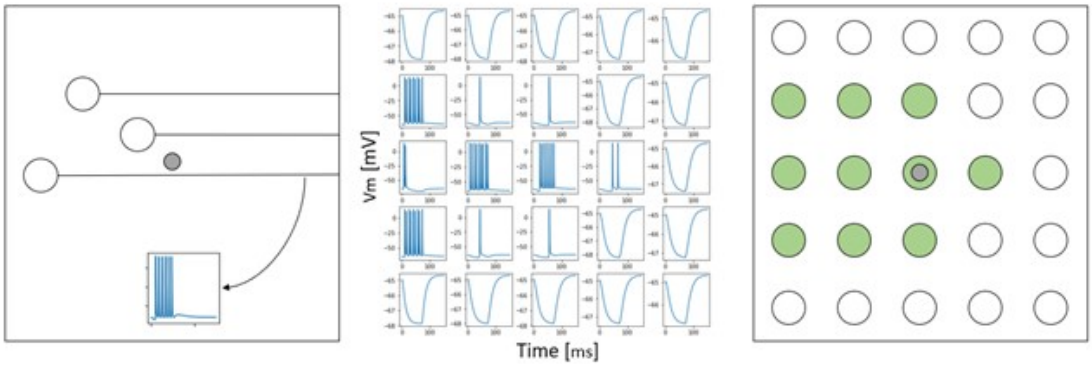

Figure 3.10: Electrical stimulation of a cells grid. The cells are placed in a regular grid, as shown on the right part of the figure. In the middle are reported spike activity of each cell, the green cells are the active ones.

The normalized firing rates due to synaptic activity show a different behaviour based on the stimulation point. Figure 3.12 shows these firing rates for a cell in the center of the lattice (position = [0,0,35]) and for cells on opposite sides (position = [130,0,35] and position = [-130,0,35]). In the epiretinal stimulation there is no considerable difference between the three cells, because the current applied was lower and the cells are activated mainly due to the electrical stimulation than due to the network activity. In the subretinal stimulation it can be observed that the normalized firing rate due to synaptic current is much higher for the central cell respect to the right and left ones. The electrode is placed closed to the retina network cells, so RGC are more influenced by the network activity than by the direct stimulation.

The combination of the effects of electrical stimulation computed trough FEM and its effects on the retinal network activation on the retinal output in terms of RC firing patterns are shown in Figure 3.13.

The firing rates are the result of the combination of synaptic current with the extracellular field due to electrode current injection. Current thresholds increase with the distance from RGC layer. The firing rate in absence of current injection is not zero, this reflects RGC spontaneous activity at rest. The cell placed at the right of the electrode requires higher currents to be activated.

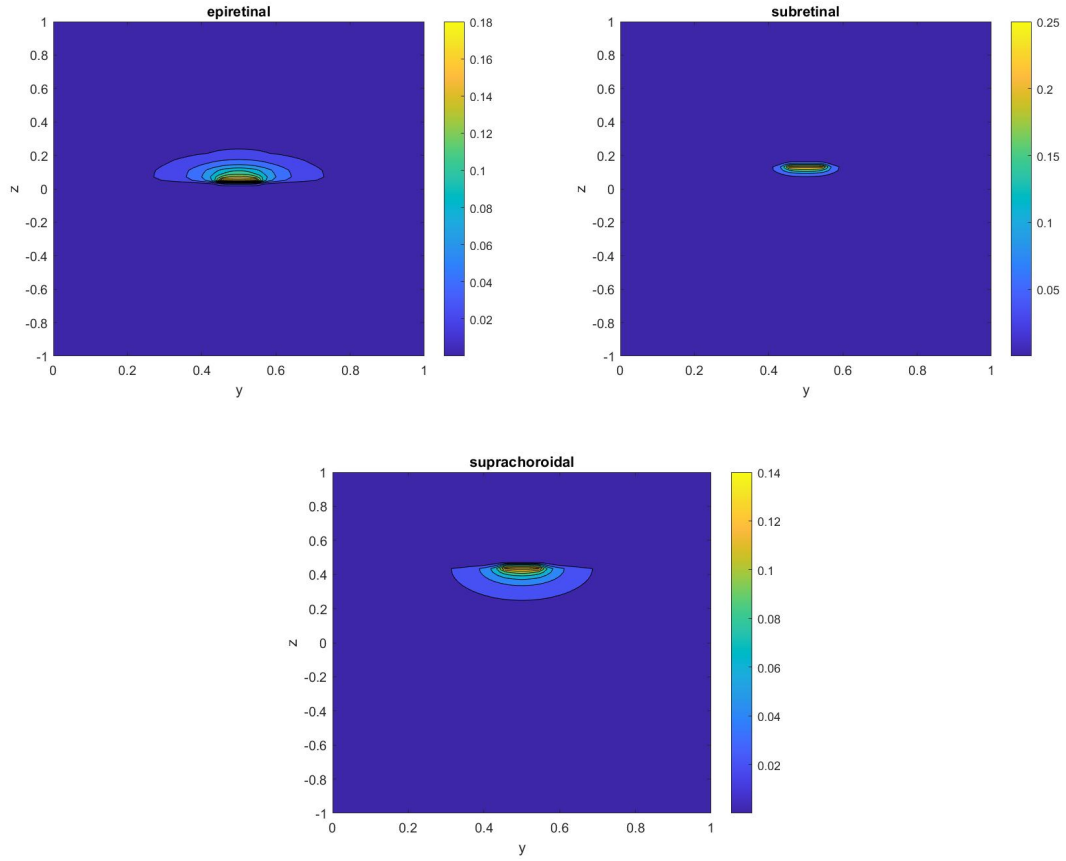

Figure 3.11: Electric potential generated through FEM, y-z plane. Epiretinal, subretinal and suprachoroidal stimulation are shown. All values are in volts. Stimulation current was set at 1 μA.

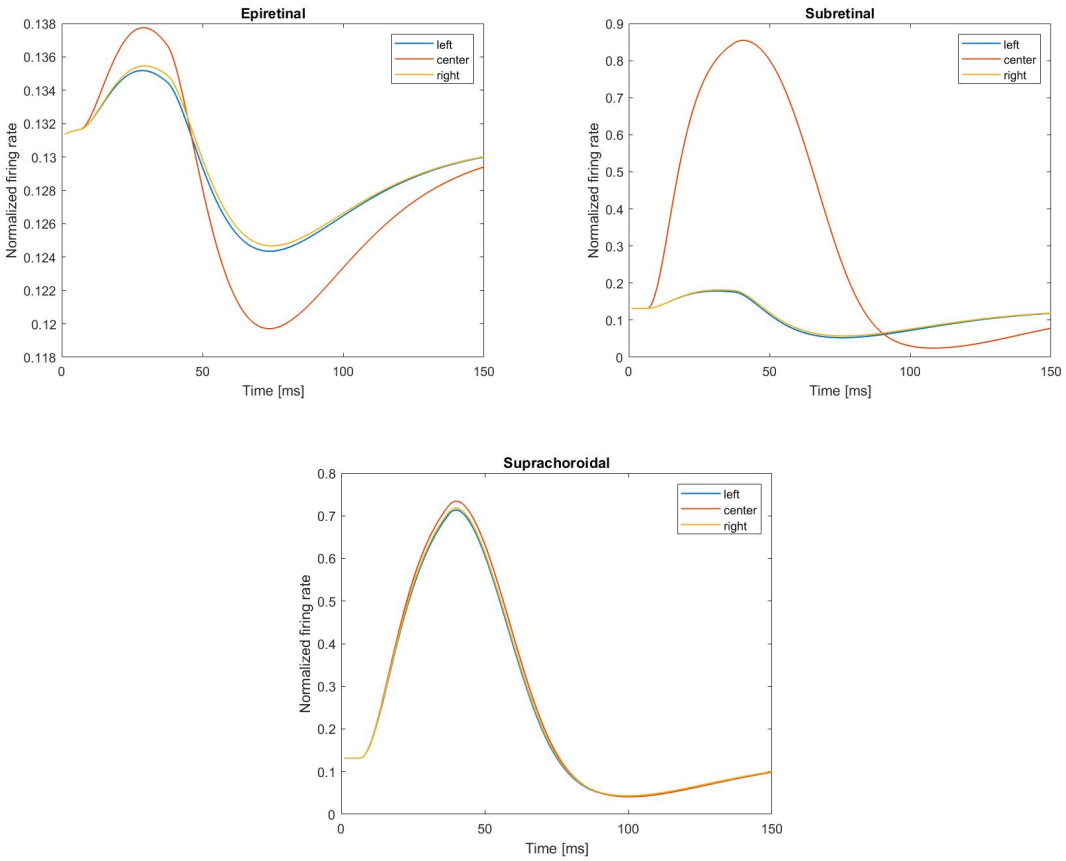

Figure 3.12: Normalized firing rate due to synaptic current for different stimulation configurations. The cell in the center is placed under the electrode, the other two are at equal distance from it, on the right and left sides. In the upper left plot we can see the result obtained with epiretinal stimulation applying a stimulation current of 0.5 µA. In the upper right plot we can see the result obtained with subretinal stimulation applying a stimulation current of 5 µA. In the lower plot we can see the result obtained with suprachoroidal stimulation applying a stimulation current of 90 µA.

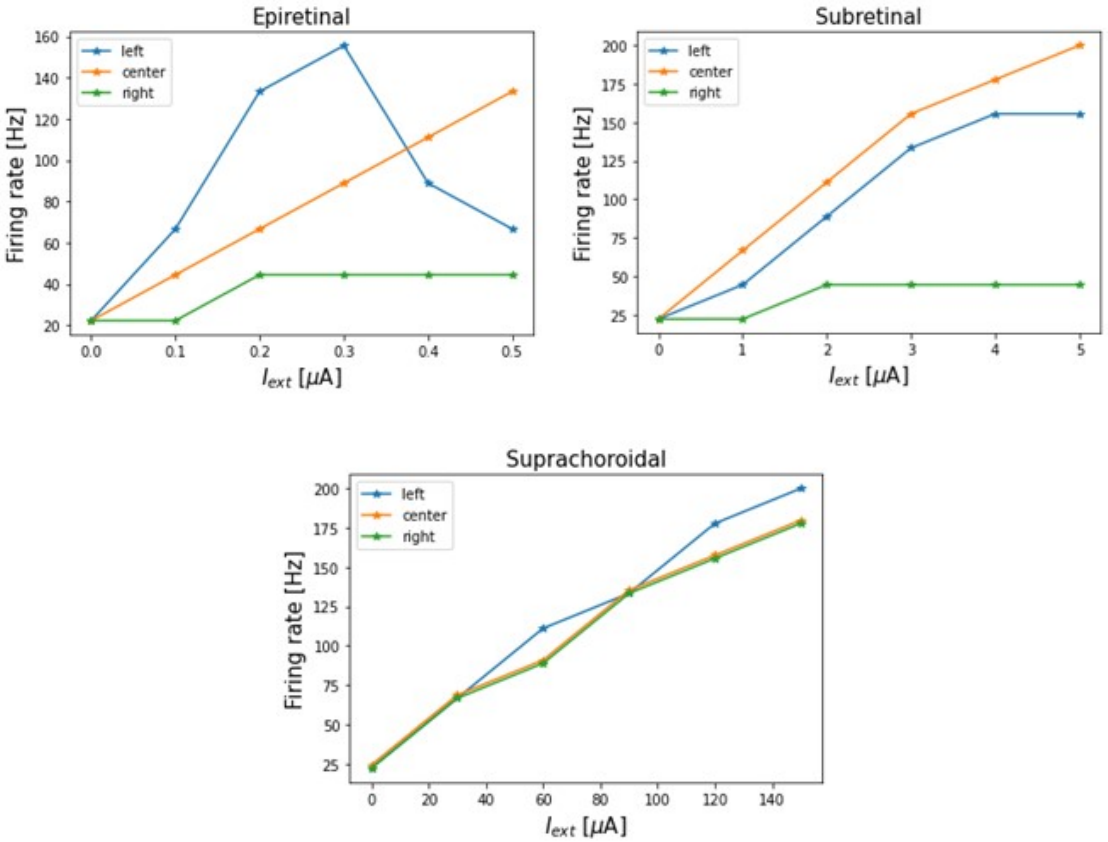

Figure 3.13: Firing rate curves for different stimulation configurations. These firing rates are the result of the contribution of electric potential generated though FEM and synaptic current obtained by the network model. The cell in the center is placed under the electrode, the other two are at equal distance from it, on the right and left sides. In the upper left plot we can see the result obtained with epiretinal stimulation. In the upper right plot we can see the result obtained with subretinal stimulation. In the lower plot we can see the result obtained with suprachoroidal stimulation.

Chapter 4

Discussion

Electrical stimulation of the retina can elicit visual perceptions in patients with retinal degeneration like RP and AMD. To improve already existing implants a better understanding of how the retina reacts to electrical stimulation is needed. In this work, we proposed a computational framework to simulate electrical stimulation of the retina considering different components: the electrical potential computed with FEM, retinal network activity, and RGC morphology.

Neuron point models do not allow us to study how cell activation changes stimulating at different points of the cell. Thus, a morphological model that considers soma and axon is necessary. This choice also allows the reproduction of different channel distributions between soma and axon. The normalized firing rate obtained with network models shows that the RGC firing rate at rest is not zero, this reflects RGC spontaneous activity that has been observed [24].

Modelling of RGC spontaneous activity is a topic of interest also in the degenerated retina, as it has been seen that with the degeneration the spontaneous activity increase until returning to normal values with the progression of the disease [25].

To add this property to the morphological model, the fictitious synaptic current injected in it is obtained from the normalized firing rate and frequency-intensity characteristic of the morphological model. From the frequency-intensity curve, it is possible to obtain the current intensity required to produce a given firing rate. The maximum firing rate value of that curve corresponds to level 1 of the normalized firing rate, while all other firing rates are computed as a percentage of the maximum value. This firing rate is then converted into a synaptic current and inserted in the model as an intracellular current. The results obtained with this choice seem reasonable, an experimental validation is needed to confirm it.

By simulating RGC electrical stimulation with the electrode placed in different positions we were able to show that the axon is activated with a lower current than the soma and when both activated it is more excitable, as reported in Figure 3.9. This agrees with findings that show a higher excitability of the axon with

respect to the soma [26]. Patient implanted with retinal prostheses reported the perception of phosphenes with an elongated shape [27]. Among the explanations of this phenomenon, the activation of axons passing under the electrode has been proposed [28]. We tried to replicate this phenomenon placing an electrode in the middle of a regular grid of RGC, studying which of them were activated by the stimulation. We showed that the stimulation activates not only the cells closer to the electrode, but also some of the farther, whose axons were in the direction of the electrode, as can be seen in Figure 3.10. Our findings support the theory that stimulation of passing axons can produce an elongated phosphene, as the brain receive a spiking activity from that cell as it were activated by the stimulation. Higher excitability of the axon and activation of passing axons prove the necessity of including RGC morphological elements into the model.

With all the components of the simulation framework we obtained results that were not predictable considering them separately, as we will now illustrate.

When simulating retinal electrical stimulation with the electrode placed at different depths of the retina, corresponding to epiretinal, subretinal and suprachoroidal implants, we saw that the retinal network reacted in different ways, influencing the final spiking of RGC. The simulations were carried out with RGC placed in three positions whit respect to the active electrode: in the center of the mosaic directly under the electrode, at the left of the electrode with the axon passing under it, and at the right of the electrode with the axon going in the opposite direction of the electrode.

We will first comment the normalized firing rate due to synaptic activity resulting from the network model in all different cases, and then consider how this influences RGC firing rates.

In epiretinal stimulation, the electrode is placed directly under RGC layer, so lower currents are needed to activate RGC. The normalized firing rates due to synaptic activity were quite low. The potential generated by current injection also reaches other cells of the network, but with a lower amplitude. Network cells will not be much activated and their influence on the RGC firing rate will be lower than the effect of the direct stimulation. There are no relevant differences between normalized firing rate of cell in the three positions, also this may be because network activity was very low.

In subretinal stimulation, the electrode is placed at photoreceptor level, close to the surviving cells of the network. This solution allows to exploit retinal processing, so network cells will have a high influence on the spiking activity of RGC, while the electrical potential generated through the stimulation that reaches RGC will be lower than the one we have with epiretinal stimulation. Our results showed that the central cell had a normalized firing rate much higher than the cells in the other positions. This may be explained by the fact that the electrode is placed in the center, so network cells in the center are more activated than the one at the

borders and the synaptic current that reaches RGC central cell is higher.

In suprachoroidal stimulation, the electrode is placed between the sclera and the choroid, further from the RGC, so higher currents should be applied to activate RGC. No relevant differences were observed in normalized firing rate of cells in different positions. It could be due to the fact that the potential before reaching the cells of the network is attenuated because of the greater distance from the electrode, and the difference between the center and the borders is not as marked as in the case of subretinal stimulation. The considerations about normalized firing rate with different implant positions will be useful to interpretate RGC firing rates.

Epiretinal stimulation results show a higher firing rate for the left cell. This is because we are stimulating the axon of the left cell and the soma of the central one, and the axon is more excitable. Moreover, synaptic current fir the three cells do not differ to affect the result.

In subretinal stimulation we see a different phenomenon, as the central cell has the highest firing rate. In this case electrical stimulation has a big influence on the network cells, mainly in the central position. So, the firing rate of the cell under the electrode is higher due to synaptic current influence. With the subretinal implant, the electrode is closer to BP, so synaptic activity has more influence than direct stimulation of RGC. If we considered only the effects of electrical stimulation, without network influence, the left cell would have the highest firing rate.

In suprachoroidal stimulation we must use higher currents to elicit RGC neural response. As we said for the synaptic currents, also the potential that reaches RGC layer does not change so much in different position of the layer, so firing rates do not show relevant differences.

The different behaviour of RGC due to stimulation at different levels implies that the combination of FEM, retinal network model and RGC morphological model is necessary to study how implants affect RGC spiking activity.

4.1 Limitations

One of the major limitations of the proposed model is the computational time needed to run the simulations. Therefore, the dimensions of the simulated retina and the duration of the simulations are limited. The retinal network model is the element more affected by this problem. To reduce it, a subsampling of the number of cells of each cell mosaics has been implemented. Although the results presented do not show a huge difference between the complete population and the subsampled one, we must consider that the stimulus was not complex. To better understand the impact of the implemented subsampling more simulation should be done, with more complex stimuli and with higher spatial frequency. We want to increase the size of the retina, but this is currently not sustainable due to computational time. We

have seen that the subsampling method helps in reducing computational time, but not enough to allow us to increase retinal size considerably. Another subsampling approach is needed. However, the subsampling we implemented allowed us to run simulations to do some test in a short time, while the results were obtained with the complete population for greater validity.

The morphological model was implemented with a limited number of segments to reduce computational time. A higher number of segments could provide more precise results, to find the best compromise between number of segments and stability of the solution a convergence analysis should be carried out.

Retinal layer thicknesses have been adapted to merge the network model with the FEM model. This parameter can change between individuals, future works should consider a way to adapt it to the specific patient.

4.2 Future work

An experimental validation of the results obtained is needed. Moreover, the influence of different electrode geometries and configurations and the effects of stimulation with intraretinal electrodes should be studied. All these elements can be easily added to the model thanks to the flexibility of the framework already implemented. Future work may also include different stimulation protocols. A lot of different patterns can be tested, changing the stimulus duration, amplitude, and phase, with combinations of cathodic and anodic currents. Study shows that after a photoreceptor degeneration RGCs are mainly intact, but the retinal network undergoes a remodelling phase [29]. Implementation of different degeneration forms could allow us to understand how this remodelling affects RGC spiking activity.

In this work only a small portion of the retina was simulated for a time duration of 150 ms, due to high computational cost. Future work should improve subsampling strategies in order to increase the retinal surface and the duration of the stimulation.

Bibliography

[1] Giacomo Valle et al. «Biomimetic Intraneural Sensory Feedback Enhances Sensation Naturalness, Tactile Sensitivity, and Manual Dexterity in a Bidirectional Prosthesis». In: *Neuron* 100.1 (2018), 37–45.e7. ISSN: 10974199. DOI: 10.1016/j.neuron.2018.08.033. URL: https://doi.org/10.1016/j.neuron.2018.08.033 (cit. on pp. 1, 7).

[2] Marco Capogrosso, Nikolaus Wenger, Stanisa Raspopovic, Pavel Musienko, Janine Beauparlant, Lorenzo Bassi Luciani, Grégoire Courtine, and Silvestro Micera. «A computational model for epidural electrical stimulation of spinal sensorimotor circuits». In: *Journal of Neuroscience* 33.49 (2013), pp. 19326–19340. ISSN: 02706474. DOI: 10.1523/JNEUROSCI.1688-13.2013 (cit. on pp. 1, 7).

[3] Cameron C. Mcintyre and Thomas J. Foutz. *Computational modeling of deep brain stimulation*. 1st ed. Vol. 116. 216. Elsevier B.V., 2013, pp. 55–61. DOI: 10.1016/B978-0-444-53497-2.00005-X. URL: http://dx.doi.org/10.1016/B978-0-444-53497-2.00005-X (cit. on pp. 1, 7).

[4] Nicolas P. Cottaris and Sylvia D. Elfar. «How the retinal network reacts to epiretinal stimulation to form the prosthetic visual input to the cortex». In: *Journal of Neural Engineering* 2.1 (2005). ISSN: 17412560. DOI: 10.1088/1741-2560/2/1/010 (cit. on pp. 2, 9).

[5] Quasar Jarosz at English Wikipedia. URL: https://en.wikipedia.org/wiki/File:Neuron_Hand-tuned.svg (cit. on p. 3).

[6] URL: https://www.moleculardevices.com/applications/patch-clamp-electrophysiology/what-action-potential (cit. on p. 4).

[7] Helga Kolb. «How the Retina Works». In: *American Scientist* 91.1 (2003), p. 28. ISSN: 0003-0996. DOI: 10.1511/2003.11.841 (cit. on p. 5).

[8] Lauren N. Ayton et al. «An update on retinal prostheses». In: *Clinical Neurophysiology* 131.6 (2020), pp. 1383–1398. ISSN: 18728952. DOI: 10.1016/j.clinph.2019.11.029. URL: https://doi.org/10.1016/j.clinph.2019.11.029 (cit. on pp. 6, 7).

[9] James D. Weiland, Wentai Liu, and Mark S. Humayun. «Retinal prosthesis». In: *Annual Review of Biomedical Engineering* 7 (2005), pp. 361–401. ISSN: 15239829. DOI: 10.1146/annurev.bioeng.7.060804.100435 (cit. on pp. 6, 7).

[10] James D. Weiland, Steven T. Walston, and Mark S. Humayun. «Electrical Stimulation of the Retina to Produce Artificial Vision». In: *Annual review of vision science* 2 (2016), pp. 273–294. ISSN: 23744650. DOI: 10.1146/annurev-vision-111815-114425 (cit. on p. 6).

[11] Jong Min Ong and Lyndon da Cruz. «The bionic eye: A review». In: *Clinical and Experimental Ophthalmology* 40.1 (2012), pp. 6–17. ISSN: 14426404. DOI: 10.1111/j.1442-9071.2011.02590.x (cit. on p. 6).

[12] Simone Romeni, Giacomo Valle, Alberto Mazzoni, and Silvestro Micera. «Tutorial: a computational framework for the design and optimization of peripheral neural interfaces». In: *Nature Protocols* 15.10 (2020), pp. 3129–3153. ISSN: 17502799. DOI: 10.1038/s41596-020-0377-6. URL: http://dx.doi.org/10.1038/s41596-020-0377-6 (cit. on pp. 7, 20).

[13] Paul Werginz and Frank Rattay. «The impact of calcium current reversal on neurotransmitter release in the electrically stimulated retina». In: *Journal of Neural Engineering* 13.4 (2016). ISSN: 17412552. DOI: 10.1088/1741-2560/13/4/046013 (cit. on p. 7).

[14] «A Multi-Domain Continuum Model of Electrical Stimulation of Healthy and Degenerate Retina». In: *Conference proceedings : ... Annual International Conference of the IEEE Engineering in Medicine and Biology Society. IEEE Engineering in Medicine and Biology Society. Annual Conference* 2018 (2018), pp. 6117–6120. ISSN: 1557170X. DOI: 10.1109/EMBC.2018.8513665 (cit. on pp. 7, 20).

[15] Paul Werginz, Vineeth Raghuram, and Shelley I. Fried. «The relationship between morphological properties and thresholds to extracellular electric stimulation in α RGCs». In: *Journal of Neural Engineering* 17.4 (2020). ISSN: 17412552. DOI: 10.1088/1741-2552/abab47 (cit. on p. 8).

[16] Shijie Yin, Nigel H. Lovell, Gregg J. Suaning, and Socrates Dokos. «A continuum model of the retinal network and its response to electrical stimulation». In: *2010 Annual International Conference of the IEEE Engineering in Medicine and Biology Society, EMBC'10* (2010), pp. 2077–2080. DOI: 10.1109/IEMBS.2010.5626300 (cit. on p. 8).

[17] Tianruo Guo, David Tsai, Siwei Bai, John W. Morley, Gregg J. Suaning, Nigel H. Lovell, and Socrates Dokos. «Understanding the retina: A review of computational models of the retina from the single cell to the network level». In: *Critical Reviews in Biomedical Engineering* 42.5 (2014), pp. 419–436. ISSN: 1943619X. DOI: 10.1615/CritRevBiomedEng.2014011732 (cit. on p. 8).

[18] P. Werginz, H. Benav, E. Zrenner, and F. Rattay. «Modeling the response of ON and OFF retinal bipolar cells during electric stimulation». In: *Vision Research* 111 (2015), pp. 170–181. ISSN: 18785646. DOI: 10.1016/j.visres.2014.12.002. URL: http://dx.doi.org/10.1016/j.visres.2014.12.002 (cit. on p. 8).

[19] Robert F. Miller, Nathan P. Staff, and Toby J. Velte. «Form and function of ON-OFF amacrine cells in the amphibian retina». In: *Journal of Neurophysiology* 95.5 (2006), pp. 3171–3190. ISSN: 00223077. DOI: 10.1152/jn.00090.2005 (cit. on p. 8).

[20] J. F. Fohlmeister and R. F. Miller. «Impulse encoding mechanisms of ganglion cells in the tiger salamander retina». In: *Journal of Neurophysiology* 78.4 (1997), pp. 1935–1947. ISSN: 00223077. DOI: 10.1152/jn.1997.78.4.1935 (cit. on p. 16).

[21] J. F. Fohlmeister, P. A. Coleman, and R. F. Miller. «Modeling the repetitive firing of retinal ganglion cells». In: *Brain Research* 510.2 (1990), pp. 343–345. ISSN: 00068993. DOI: 10.1016/0006-8993(90)91388-W (cit. on p. 16).

[22] J. F. Fohlmeister and R. F. Miller. «Mechanisms by which cell geometry controls repetitive impulse firing in retinal ganglion cells». In: *Journal of Neurophysiology* 78.4 (1997), pp. 1948–1964. ISSN: 00223077. DOI: 10.1152/jn.1997.78.4.1948 (cit. on p. 16).

[23] R. J. Greenberg, T. J. Velte, G. Scarlatis, and E. De Juan. «A computational model of extracellular electrical stimulation of the retinal ganglion cell». In: *Investigative Ophthalmology and Visual Science* 37.3 (1996), pp. 505–514. ISSN: 01460404 (cit. on pp. 19, 20).

[24] David J. Margolis and Peter B. Detwiler. «Different mechanisms generate maintained activity in ON and OFF retinal ganglion cells». In: *Journal of Neuroscience* 27.22 (2007), pp. 5994–6005. ISSN: 02706474. DOI: 10.1523/JNEUROSCI.0130-07.2007 (cit. on p. 38).

[25] Chris Sekirnjak, Clare Hulse, Lauren H. Jepson, Pawel Hottowy, Alexander Sher, Wladyslaw Dabrowski, A. M. Litke, and E. J. Chichilnisky. «Loss of responses to visual but not electrical stimulation in ganglion cells of rats with severe photoreceptor degeneration». In: *Journal of Neurophysiology* 102.6 (2009), pp. 3260–3269. ISSN: 00223077. DOI: 10.1152/jn.00663.2009 (cit. on p. 38).

[26] Maarten H.P. Kole and Greg J. Stuart. «Is action potential threshold lowest in the axon?» In: *Nature Neuroscience* 11.11 (2008), pp. 1253–1255. ISSN: 10976256. DOI: 10.1038/nn.2203 (cit. on p. 39).

[27] Michael Beyeler, Ariel Rokem, Geoffrey M. Boynton, and Ione Fine. «Learning to see again: Biological constraints on cortical plasticity and the implications for sight restoration technologies». In: *Journal of Neural Engineering* 14.5 (2017). ISSN: 17412552. DOI: 10.1088/1741-2552/aa795e (cit. on p. 39).

[28] Michael Beyeler, Devyani Nanduri, James D. Weiland, Ariel Rokem, Geoffrey M. Boynton, and Ione Fine. «A model of ganglion axon pathways accounts for percepts elicited by retinal implants». In: *Scientific Reports* 9.1 (2019), pp. 1–16. ISSN: 20452322. DOI: 10.1038/s41598-019-45416-4 (cit. on p. 39).

[29] Bryan W. Jones and Robert E. Marc. «Retinal remodeling during retinal degeneration». In: *Experimental Eye Research* 81.2 (2005), pp. 123–137. ISSN: 00144835. DOI: 10.1016/j.exer.2005.03.006 (cit. on p. 41).